

Evaluation of Fiber Optic Technology for Advanced Reactor Instrumentation

Undergraduate Honors Thesis

Presented in Partial Fulfillment of the Requirements for
Graduation with Distinction
at The Ohio State University

By

John P. Hanson

* * * * *

The Ohio State University

2010

Defense Committee:

Professor Thomas Blue, Advisor

Professor Don Miller

Approved by

Advisor

Undergraduate Program in Mechanical
Engineering

Copyrighted by

John P. Hanson

2010

ABSTRACT

The harsh, high temperature, high radiation environment of next generation nuclear reactors will require new sensor technology to accurately monitor their operating conditions, and one potential technology for such sensors is that of fiber optics. Previous work has shown that fiber optics have promising ability to withstand these harsh conditions, in particular single-crystal sapphire fibers, which can withstand much higher temperatures than traditional silica fibers. However, they have not been extensively tested in a combined high temperature, high radiation environment, and the competing effects of radiation damage and annealing within both types of fiber are not well understood. It has been hypothesized that in these conditions sapphire-based fiber optic sensors will provide survivability superior to silica-based fibers, and numerous advantages over traditional electrical sensors. The goal of this project was to design a furnace needed to test this hypothesis, as well as gain preliminary data on the survivability of silica-based fibers. A furnace was designed to be operated inside a dry tube experimental facility at the OSU Research Reactor, allowing simultaneous irradiation and heating of the fibers while monitoring them *in situ*. A prototype was constructed of this design for preliminary testing, providing experience with the construction and instrumentation of the device. This experience has also helped to validate the feasibility of the furnace design. In addition, the prototype has been used to gather valuable data on the effects of temperature on silica-based fibers, providing a baseline of comparison for future sapphire fiber testing. As expected, this testing has confirmed the limitations of silica-fibers at high temperatures, and the need to analyze more robust

solutions such as sapphire based fibers. Due to the initial success of the prototype, the construction of the new furnace will soon proceed, enabling future studies of sapphire based fibers.

ACKNOWLEDGMENTS

I would like to thank many people for their help with this project. Dr. Thomas Blue and Dr. Don Miller have provided outstanding guidance over the past few years as I became acquainted with their research lab, and finally got involved in this particular project. Dr. Blue has been supportive of my growth as both a student and a researcher since I joined the lab, and has been more than patient as I continued to try to find a balance between these two pursuits. David Hawn deserves credit for helping me at nearly every turn along the way, being both instrumental in helping me with my work on this specific project, and in helping me to become a better researcher during my time in the lab. He has been a great mentor as well as friend. I also could not have done this project without the love and support of my parents, Marianne and Peter Hanson, my friends, and especially my girlfriend Lindsey Pack, who has been the encouraging voice that has kept me going throughout.

TABLE OF CONTENTS

ABSTRACT.....	ii
ACKNOWLEDGMENTS	iv
TABLE OF CONTENTS.....	v
LIST OF FIGURES	vii
Chapter 1: INTRODUCTION.....	2
1.1 Introduction.....	2
Chapter 2: Background	5
2.1 Fiber Optic Sensors.....	5
2.1.1 External Fabry Perot Interferometric Sensors	6
2.1.2 Fiber-Bragg Gratings	14
2.2 Effects of Heating Fiber.....	17
2.3 Summary.....	22
Chapter 3: Methods.....	24
3.1 High Temperature Furnace Design.....	24
3.1.1 Sapphire Fiber Specification.....	25
3.1.2 Heater Specifications	26
3.1.3 Heater Instrumentation.....	28
3.1.4 Furnace Structure	29
3.1.5 Control System.....	32
3.2 Furnace Prototype.....	32
3.2.1 Prototype Heater	33
3.2.2 Prototype Heater Controller	33
3.2.3 Prototype Furnace Instrumentation.....	35
3.2.4 Prototype Furnace Structure	41
3.2.5 Prototype Furnace Insulation	41
3.2.6 Prototype Optical Equipment.....	43
3.2.7 Prototype Fiber Connectors	43
3.3 Silica Fiber Testing Procedures	45
3.3.1 General Fiber Testing Procedures.....	45

3.3.2 Repeating Previous Experiment by Toossi and Modarress	45
3.3.3 Prototype Testing at Increasing Temperatures.....	46
3.4 Summary.....	47
Chapter 4: Results	48
4.1 Prototype Furnace Silica Fiber Testing	48
4.1.1 Repeating Previous Experiment.....	48
4.1.2 Higher Temperature Testing, With Connectors.....	50
4.2 Physical Damage to Fibers	53
Chapter 5: Analysis.....	55
5.1 Optical Performance of Silica Fibers.....	55
5.1.1 Optical Testing.....	55
5.1.2 Lessons Learned from Optical Testing	60
5.2 Physical Performance of Silica Fibers.....	60
5.3 Summary.....	61
Chapter 7: CONCLUSIONS AND FUTURE WORK	63
7.1 Conclusions	63
7.2 Future Work.....	63
7.2.1 Short Term	63
7.2.2 Long Term	64
Bibliography	65
Appendix.....	67
Appendix A: CAD Drawings of Initial Furnace Design.....	68
Appendix B: Ocean Optics LS-1 Manufacturer's Specifications	74
Appendix C: Ocean Optics USB 2000 Manufacturer's Specifications	75

LIST OF FIGURES

Figure 1: Schematic of EFPI Sensor	6
Figure 2: Schematic of Alternative EFPI Sensor	8
Figure 3: Illustration of Signal Fading in EFPI Sensors	9
Figure 4: Quadrature Phase Shifted EFPI Sensor Output	10
Figure 5: Interference Pattern for White Light Interferometry	12
Figure 6: Schematic of Data Acquisition System Using Fiber Pro 2	13
Figure 7: Calibration Curve for Luna EFPI Temperature Sensor	14
Figure 8: Schematic of Fiber-Bragg Grating and Typical Spectral Response	16
Figure 9: High Temperature Effects in Aluminum Coated, Germanium Doped Fiber	19
Figure 10: Properties of Fibers in Toossi and Modarress Experiment	20
Figure 11: Effect of Temperature on Fiber Degradation, Toossi and Moddarress Experiment ...	21
Figure 12: Schematic of Tube Furnace from MHI	27
Figure 13: Example Robust Radiator Heater from MHI	28
Figure 14: Initial CAD design for High Temperature Furnace	30
Figure 15: Digi-Sense Temperature Controller	34
Figure 16: Omega Thermometer for Backup Thermocouple	35
Figure 17: Initial Attempt at Locating Thermocouples	36
Figure 18: Four Bore Ceramic Insulator	38
Figure 19: Attaching Ceramic Insulators to Steel All-thread	39

Figure 20: Final Layout of Thermocouples in Prototype Design	40
Figure 21: Ceramic Tiles Used as End-Caps for Prototype Heater	42
Figure 22: Bullet Bare Fiber Adapter	44
Figure 23: Prototype Testing, 325 °C.....	49
Figure 24: Prototype Testing, 325 °C, Additional Wavelengths.....	50
Figure 25: Prototype Testing, 750 °C.....	51
Figure 26: Prototype Testing, 750 °C, Additional Wavelengths.....	52
Figure 27: Prototype Testing, 750 °C Prolonged Test	53
Figure 28: Physical Damage to Fiber, Prototype Heater Testing at 750 °C	54
Figure 29: Physical Damage to Fiber, Prototype Heater Testing at 750 °C, Close-Up.....	54
Figure 30: Introduction of Light from Secondary Source in Fibers	58
Figure 31: Variation of Secondary Source Radiation Signal, Oikari Study	59

CHAPTER 1: INTRODUCTION

1.1 Introduction

As the development of Generation IV nuclear power plants continues, advanced instrumentation will be an important focus area of research. Nuclear reactors present very difficult instrumentation challenges, due to the high temperature, high radiation environment faced by sensors during in-core operation, and advanced reactors will continue to push the limits of available instrumentation technology. One technology in particular that has the potential to greatly improve reactor instrumentation is that of fiber optics. Fiber optics present a variety of favorable characteristics for such applications, including immunity to electromagnetic interference that plagues electrical sensors, the wavelength-encoded nature of the signal, and their small size and flexibility. The wavelength-encoded nature of the signal provides resistance to signal drift due to darkening of the fiber, as the measurement depends on wavelength rather than strength of the signal. These favorable characteristics, in addition to the wide variety of different types of fiber optic sensors available, make fiber optic based instrumentation a strong candidate for implementation in nuclear reactor environments.

Before this technology can be applied to reactor instrumentation, it is crucial that the behavior of optical fibers in this harsh environment be well understood, as such instrumentation would ideally be capable of surviving entire refueling cycles of 18 or more months. Silica optical fibers have shown high potential for use in these environments, but they have not been

subjected to conditions as harsh as those that would be faced during extended in-core operation. The fibers have been tested at high temperatures, approaching 1000°C, and in moderate radiation environments, but they have not been tested under intense radiation at very high temperatures. This issue is being addressed by current work in the lab of Dr. Thomas Blue, in which an experiment is being designed to subject silica optical fibers to high temperatures and high radiation at the Ohio State University Research Reactor. The goal is to model, as well as measure, the performance of the fibers in this environment, and pave the way for future optical sensors employing these fibers.

One of the biggest limitations on silica optical fibers is that they are typically unable to operate at temperatures exceeding 900°C. This is due to their degraded mechanical strength, as well as thermal diffusion of the dopant and re-crystallization of the glass. Single-crystal sapphire optical fibers present a potentially higher performance alternative to silica fibers, with one major advantage being a melting point of greater than 2000°C. In addition to their high melting point, the fibers have a variety of other potential benefits, which include increased radiation resistance, and a lack of dependence on cladding and coating, without which silica fibers become very brittle and difficult to handle. Like silica fibers, single-crystal sapphire fibers have been tested to their limits at high temperatures, and have been subjected to moderate radiation, but have not been studied in a combined high temperature, high radiation environment that approaches the harsh conditions they would face during in-core operation in a nuclear reactor. There is still much to be learned about these fibers before they can be used in advanced instrumentation applications in this setting, and the ability to test the fibers in such an environment is a necessary first step in learning how they will behave.

In addition to designing an experiment to test these sapphire fibers, this project was concerned with examining the effects of high temperature on silica fibers, as a first step towards the completion of a larger study on these fibers. This was accomplished by constructing a prototype of the sapphire furnace, with a design analogous to that of the sapphire furnace, using a lower temperature heater and other equipment already available in the lab. This process not only allowed important lessons to be learned prior to the construction of the higher temperature heater, but it provided useful operating data that will serve as a baseline for future testing of silica fibers in the lab. Next steps will be to construct two additional furnaces, one for silica fiber testing, not discussed in this paper, and the other for higher temperature testing of sapphire fibers, as described in the Methods section of this report. Both of these heaters will allow real-time monitoring of fiber performance while operating at high temperature in a radiation environment at the OSU Research Reactor.

CHAPTER 2: BACKGROUND

Fiber optic instrumentation presents a variety of potential advantages over current instrumentation technologies. These advantages, including immunity to electrical noise and magnetic fields, as well as the wavelength-encoded nature of the signal, are a direct result of the unique characteristics of fiber optic cables and the creative application of these principles to various types of sensor designs. By taking advantage of these characteristics, and the correct types of fiber optic sensors, it is hoped that a new generation of reactor instrumentation, with superior durability and other unique advantages, can be created. Rather than provide an overview of light guides, fiber optics, and their properties in this Thesis, the reader is referred to the literature such as *An Introduction to Optical Fibers*, by Cherin, for the necessary background on the subject. An overview of fiber optic sensing technology, as well as the effects of heating silica fibers to high temperatures, will be included here.

2.1 Fiber Optic Sensors

There are a variety of different fiber optic sensing technologies that have the potential to be advantageous in nuclear reactor instrumentation. Two types of sensors in particular will be considered here. Both share common characteristics that offer significant advantages over traditional electrical sensors, while each operates on different principles. The first type of sensor is known as the Extrinsic Fabry Perot Interferometric (EFPI) sensor, and it operates using optical

interferometry. The second, called the Fiber-Bragg Grating (FBG), operates on the principle of photosensitivity.

2.1.1 External Fabry Perot Interferometric Sensors

Optical interferometers such as EFPI sensors operate using interference between multiple beams of light. A reference beam of light interferes with a sensing beam, and the resulting interference pattern is used to obtain information about some external parameter. In a basic EFPI sensor, a Fabry-Perot cavity is created by sealing two fibers together, with a small air gap between them, inside a hollow tube, as shown in Figure 1, below.

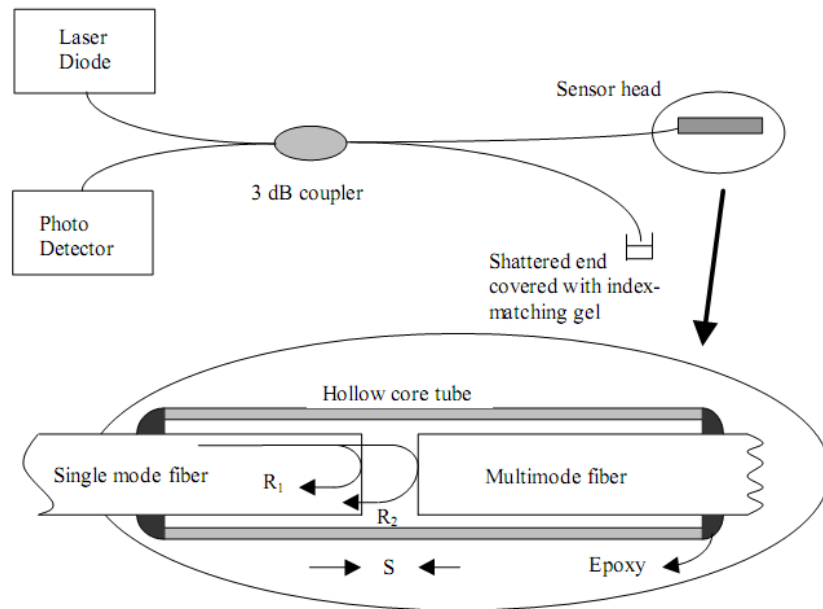


Figure 1: Schematic of EFPI Sensor

The first fiber, a single-mode fiber, is the input/output fiber, and the reference signal beam, R_1 , is input into this fiber. At the interface between the single-mode fiber and the air gap the

reference beam is partially reflected back down the single-mode fiber. The remainder of the beam, R2, reflects off of the second fiber, a multi-mode fiber, and returns down the single-mode fiber as well. This beam interferes with the reference beam, creating an interference pattern which is dependent on the path length difference between the two. This interference pattern can be measured using a photo detector, and changes in the pattern can be used to determine changes in the length of the air gap between the two fibers. These changes can then be related to external variables such as pressure, temperature, or strain, which all predictably alter the length of the air gap, thus allowing the sensor to be used to measure these variables.

A similar sensor can be created by affixing a chip on the end of a fiber, in which the length of the chip is analogous to the length of the air gap in the sensor above. In this case the chip is made out of an optically permeable material, and the reference beam reflects off of the interface between the fiber and the chip, while the remainder of the beam reflects off of the other end of the chip, returning through the fiber as before. Just as in the above sensor, the two beams create an interference pattern, and this pattern is used to measure external stimuli. For example, the length of the chip would vary according to its temperature, some pressure acting on the sensor, or other stimuli. This type of sensor is illustrated in Figure 2, below.

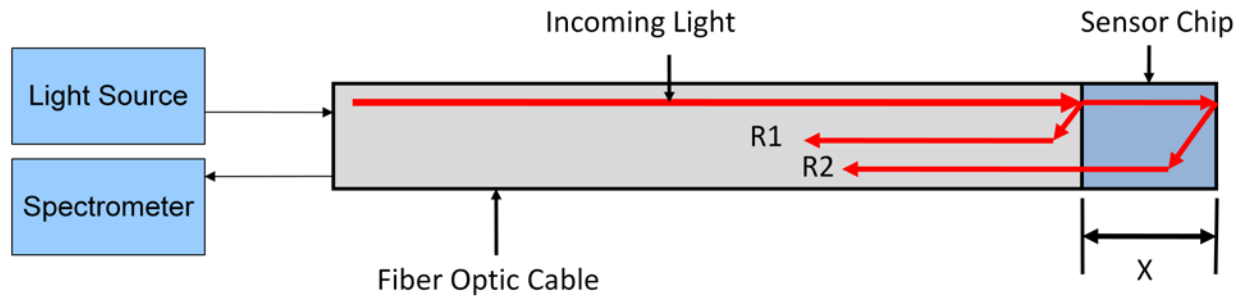


Figure 2: Schematic of Alternative EFPI Sensor

Both types of EFPI sensors operate on the same optical principles, and are interrogated using the same methods. There are a variety of different means of interrogating the sensors, each with its own advantages and disadvantages. The most basic method uses a single wavelength laser. This method requires the most basic equipment, but it is plagued by difficulties with ‘signal fading,’ due to the nature of the output signal. The output of the EFPI sensors varies sinusoidally with changes in the length of the air gap, resulting in maximums and minimums in the sensitivity of the device. As shown in Figure 3, below, the result is that an external perturbation causing a change in gap length of ΔL will cause changes in the output of very different magnitude depending on the operating point of the sensor. The signal is said to ‘fade’ as the sensitivity decreases at the minimum and maximum output.

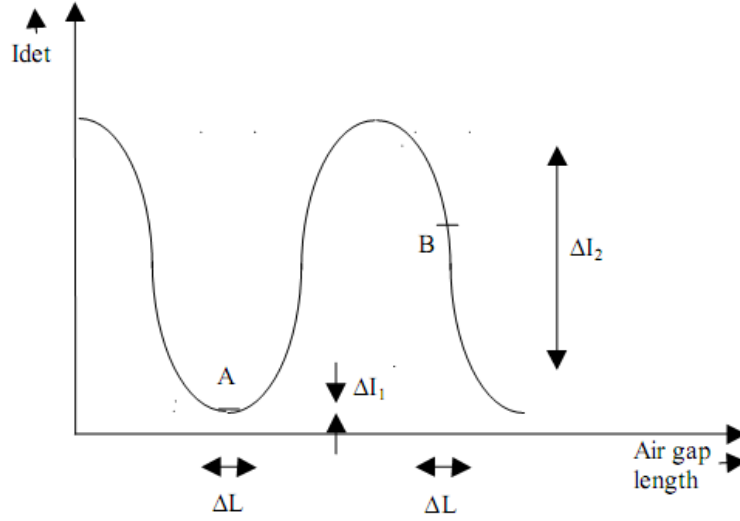


Figure 3: Illustration of Signal Fading in EFPI Sensors

Comparing the magnitudes of ΔI_1 and ΔI_2 one can see the difficulty in using these sensors when the operating point is located on an insensitive range. In addition, as the periodic nature of the output suggests, interrogating the sensors in this way can only give a relative gap length, as the output signal will be equivalent for a gap length of L and a gap length of $L+\lambda$. The result is that only relative changes in the gap length can be detected, and the sensor has a limited range over which it can operate.

There are a variety of alternative means of utilizing EFPI sensors that help to mitigate the effects of signal fading, and even a method that can be used to determine the absolute gap length rather than simply a relative gap length. The first is called Quadrature Phase Shifted demodulation. Here two different sensors are used, and their outputs are intentionally set 90° out of phase. The resulting outputs are shown in Figure 4, below, for comparison to the base case, in Figure 3 above.

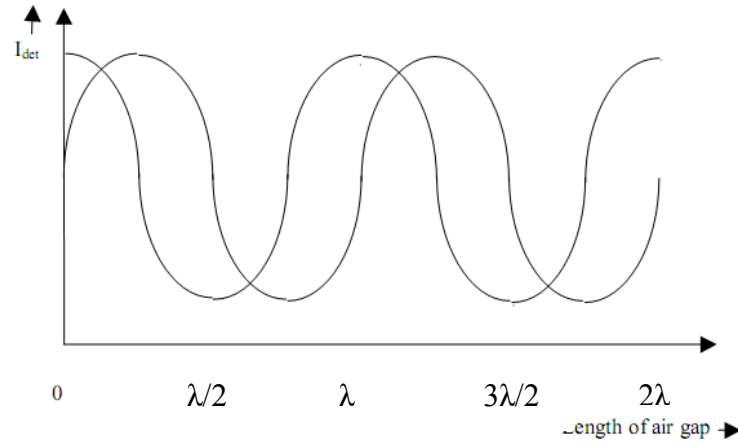


Figure 4: Quadrature Phase Shifted EFPI Sensor Output

This system guarantees that when one sensor is operating in a range of low sensitivity, the other is operating at high sensitivity. The advantage is that much more accurate measurements can be made using the QPS system. The increased accuracy comes at a cost of complexity, however, as the sensors must be much more carefully fabricated, complex signal processing is involved, and there is some difficulty to maintaining the 90° offset through repeated measurements. In addition, this method does not yet solve the issue of relative vs. absolute gap length, and the operating range is still limited as a result.

Another method for measuring the change in air gap length is to use a single sensor, with two wavelengths of light. This method, known as the Dual Wavelength method, allows the straightforward calculation of the relative gap length. Equations 1.1-1.2, below, are used to calculate the change in output signal phase for each wavelength, λ , where L is the length of the air gap.

$$\Delta\Phi_1 = \frac{4\pi L}{\lambda_1} \quad (1.1)$$

$$\Delta\Phi_2 = \frac{4\pi L}{\lambda_2} \quad (1.2)$$

The relative phase difference between the two signals is calculated using Equation 1.3, below.

$$\Delta\Phi = 4\pi L \frac{\Delta\lambda}{\lambda_1\lambda_2} \quad (1.3)$$

The advantage of this approach is that it requires less complexity than the QPS approach. The disadvantage, similar to the above methods, is that the dynamic range of the sensor is limited to $0 < \Delta\Phi < \pi$ radians.

Perhaps the most effective method for interrogating these sensors is the use of White Light Interferometry. This method has many advantages over laser-based sensors, including higher accuracy, higher resolution, a larger dynamic measurement range, and immunity to optical power fluctuations (Han). In this method, the sensor is illuminated using a broadband LED light source rather than lasers of specific wavelengths, and the output is analyzed using an optical spectrum analyzer. There are a variety of possible signal demodulation methods, and Han explains some of the pros and cons of these methods. The basic principle, however, is that for any wavelength at which the reference and sensing beam exhibit a phase difference of 2π , the beams interfere constructively, and show up as a peak in the output spectrum. By finding two

consecutive peaks in the spectrum, at wavelengths λ_1 and λ_2 , one can calculate the absolute gap length using Equation 1.4, below.

$$L = \frac{\lambda_1 \lambda_2}{2(\lambda_1 - \lambda_2)} \quad (1.4)$$

An example interference pattern is provided below, as Figure 5, to illustrate the constructive interference, and the choice of consecutive wavelengths for use in Equation 1.4 above (Bhatia).

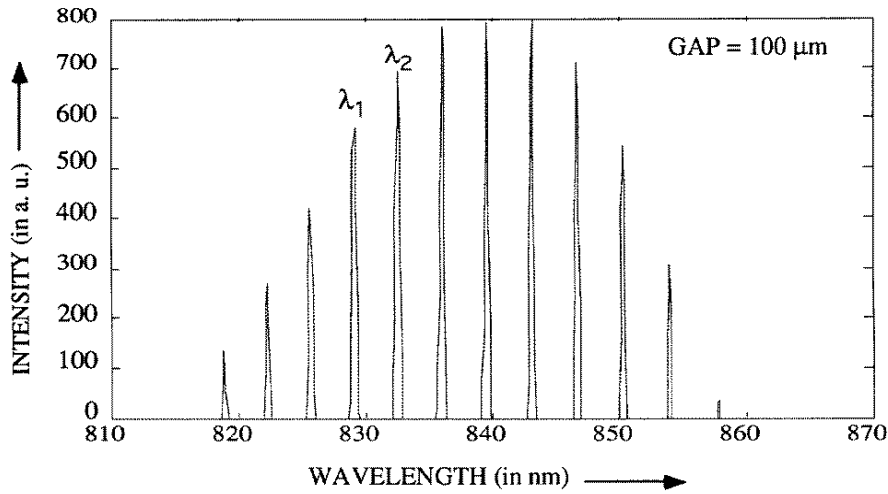


Figure 5: Interference Pattern for White Light Interferometry

As described above, this method, and other white light interferometry methods, provide many advantages over methods using lasers, but the cost of such advantages is the need for more expensive equipment.

Our group has basic experience with the use of EFPI sensors, testing a commercial system from Luna Innovations on loan from Dr. Xiaodong Sun. This system utilizes white light

interferometry, and can be used with any EFPI sensors, but our testing was done on the second type of sensor described above, those with a sensor chip attached to the end of a fiber. The system, called the Fiber Pro 2, is a self-contained broadband LED source, spectrum analyzer, and A/D converter. It connects to a PC using USB, and the included software can then be used to demodulate the signal, convert the measured gap length to temperature data, and store this data for future use. Figure 6, below, shows a schematic of a data acquisition system using the Fiber Pro 2.

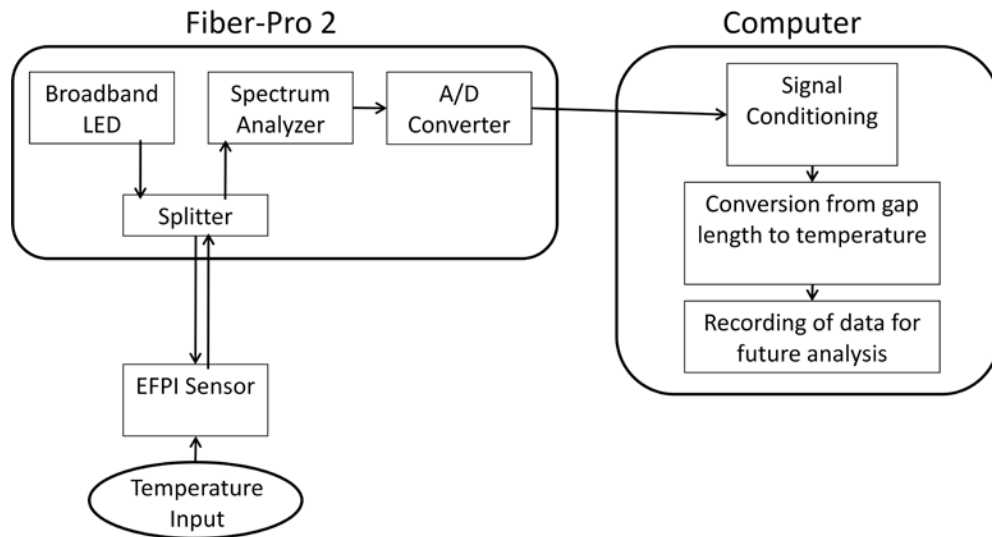


Figure 6: Schematic of Data Acquisition System Using Fiber Pro 2

Temperature sensors provided by Luna come with “calibration coefficients” provided, which are unique to each sensor, and must be input into the data acquisition software to convert data on absolute gap length to a temperature. While testing the system it was determined that the sensor was no longer correctly calibrated, and through trial and error it was determined that the

calibration coefficients were simply the coefficients of a third-order polynomial curve fit to the temperature vs. absolute gap length data. With this knowledge we were able to manually calibrate the sensor using an oven to heat the sensor, and a simple type K thermocouple of known accuracy to measure the temperature. The resulting curve fit is shown in Figure 7 below. Though the calibration is not accurate to more than a few degrees, this allowed us to gain insight into the calibration process, and made the sensor usable again, as the previous calibration suffered from a large enough error as to make the temperature sensor unusable.

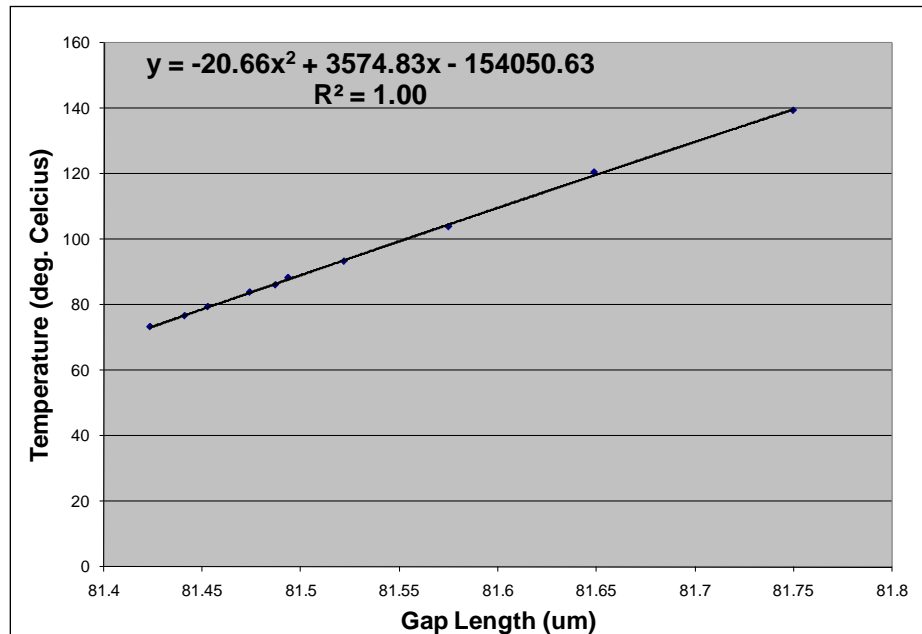


Figure 7: Calibration Curve for Luna EFPI Temperature Sensor

2.1.2 Fiber-Bragg Gratings

Another type of fiber-optic sensor that presents particularly valuable characteristics for reactor instrumentation is called the Fiber-Bragg grating (FBG). This type of sensor was first

made possible with the discovery of photosensitivity in 1978 at the Communication Research Center in Canada (Othonos and Kalli). Photosensitivity refers to a permanent change in the index of refraction of the fiber core when exposed to light with a characteristic wavelength and intensity. The appropriate wavelength and intensity is specific to the type of fiber being used, and it has been found that many types of fibers exhibit photosensitivity. Initially these index of refraction changes were created using laser light launched into the core, but later it was discovered that they could be etched into the fiber from the side, using UV light. Fibers are irradiated using a periodic pattern created by two 244-nm beams, which results in a periodic change in the index of refraction within the core (Othonos and Kalli). The period can be altered by changing the angle between the beams, and this periodic change in the index of refraction is the key to FBG sensors.

Rather than measuring the length of a sensor chip, or an air gap outside the fiber, as with EFPI sensors, FBG sensors are etched directly into the fiber as described above. They consist of a periodic change in the index of refraction of the fiber, and operate by reflecting a specific wavelength of light, known as the Bragg wavelength, determined by the period of the grating. Figure 8, below, shows a basic representation of an FBG, and the way it reflects a particular wavelength of light, while transmitting the rest (Othonos and Kalli).

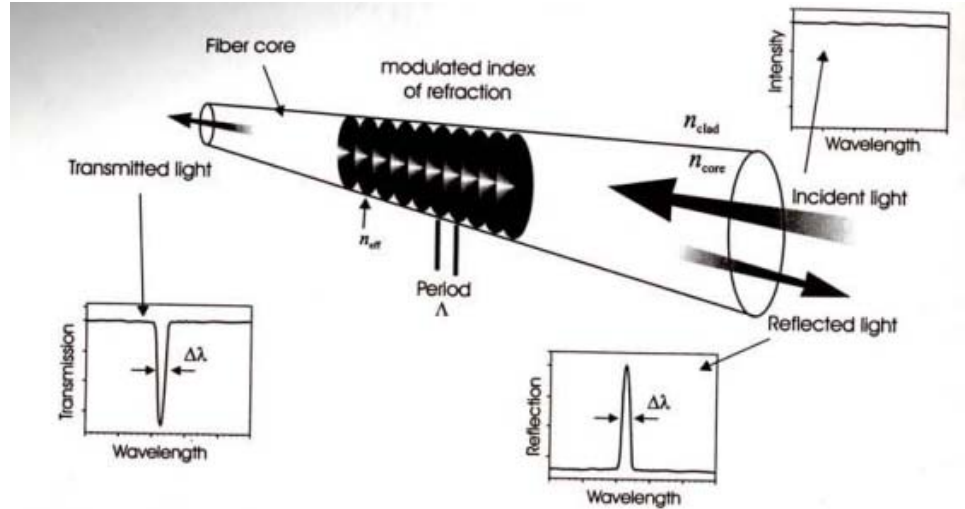


Figure 8: Schematic of Fiber-Bragg Grating and Typical Spectral Response

As the fiber is heated, or strained, the period of the grating changes, resulting in a change in the reflected wavelength. In this way, the grating can be used as a sensor for a variety of external stimuli. Though the stimulus that is being measured is very similar to that in the case of the EFPI sensors, the way in which it is measured is very different. Instead of attempting to determine the amount that the air gap, or chip, has changed in length by using interference patterns, one need only monitor the reflected wavelength of the FBG to interrogate the sensor.

In addition, FBG sensors provide a variety of other advantages over other types of fiber optic sensing technologies. One advantage is that etching the sensors directly into the fibers eliminates the need for additional fiber optic components, thereby decreasing the size and complexity of the system. Another advantage, which is particularly important to applications in reactor instrumentation, is the ability to multiplex the sensors, and create a quasi-distributed sensor network using FBG's. There are a variety of techniques that can be used to multiplex the

sensors that allow multiple measurements to be taken along the same fiber. The first and most easily implemented technique is called Wavelength Division Multiplexing (WDM). In WDM each sensor is encoded with its own Bragg wavelength, such that multiple FBGs can be interrogated on the same fiber. This technique is limited by the usable range of wavelengths within a fiber, and by the temperature dependence of the Bragg wavelength. For example, if a fiber has a usable range of just 100 nm in which FBG sensors can be created, and the Bragg wavelength of a specific grating can shift over a range of 10 nm, this technique can result in a maximum of ten gratings per fiber. To maximize the number of FBG sensors on a single fiber, an additional technique, Time Division Multiplexing (TDM) can be used in conjunction with WDM. In TDM, sensors are interrogated based on timing, and in this way multiple sensors with the same Bragg wavelength can be distinguished on one fiber, multiplying the number of sensors possible using WDM. Due to the nature of TDM, each FBG must be only partially reflective, so that some fraction of the light at each wavelength continues to the next sensor. These multiplexing techniques can be used in conjunction with a branching system in which multiple fibers are used, with the end result being a great many distinct measurements being taken with a relatively compact and unobtrusive system.

2.2 Effects of Heating Fiber

The primary motivation for testing single-crystal sapphire fibers as opposed to silica fibers is the significantly increased temperature range of these fibers. Silica fibers simply cannot withstand temperatures greater than 1000 °C, and in many aspects cannot survive at temperatures nearly this high. The primary negative effect of high temperatures on silica fibers is the

destruction of the fiber coating, or the protective outside layer, as described in the above section. In fibers typically used for telecom applications the coating is limited to about 180 °C, while high temperature polyimide coatings can survive temperatures of about 385 °C (Wang, Zhu and Pickerell). The destruction of the coating does not necessarily have a negative effect on the optical properties of the fiber, but leaves the fibers brittle and weak. Higher temperatures can be achieved using various metallic coatings, such as gold or aluminum. For example, Shiota and Hidaka show that an aluminum coating allows fibers to maintain their mechanical strength even at high temperatures, and using a germanium-doped fiber they are able to produce very good optical properties at temperatures up to 650 °C (Shiota and Hidaka). Figure 9, below, shows the spectral loss change in these fibers from 25 °C to 650 °C. It is interesting to note that the process of coating the fibers in aluminum induces stresses in the fiber known as microbending, which actually decrease with temperature, resulting in high losses below 100 °C, and much-improved properties at higher temperature.

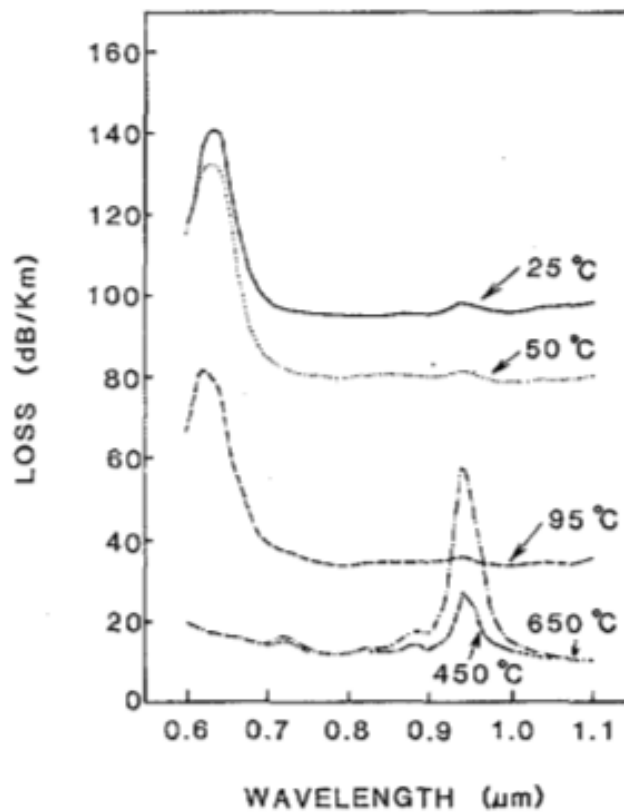


Figure 9: High Temperature Effects in Aluminum Coated, Germanium Doped Fiber

Also of note in Figure 9 is the absorption peak that occurs at around 0.95 μm . Although the ability of the coating to withstand higher temperatures offers a greater operating range of the fibers, they are still limited by optical losses caused by three main components. The first is the thermal diffusion of waveguide-defining dopants in the fiber, the second is crystallization of the glass, and the final factor is the softening of the glass under stress (Wang, Zhu and Pickerell). In this case, the absorption peak is from the thermal diffusion of OH. Another study, by Toossi and Modarress, shows the effect of temperature on three different fluorine-doped silica fibers. Figure 10, below, provides the properties of each of these fibers, which were heated to 320 $^{\circ}\text{C}$, and

monitored at wavelengths of 589 nm and 764 nm using light sources with sodium and potassium filters. Figure 11, below, shows the attenuation in the fibers at each wavelength over the course of the heating and cooling cycle (Toossi and Modarress).

- 1) Polymicro FHP 200/240/300.
This is a high OH step-index synthetic fused silica core with fluorine-doped silica cladding. It has a polyimide buffer capable of withstanding temperatures of -100 to $+360^{\circ}\text{C}$.
- 2) Fiberguide SFS200/240A.
This is also a high OH step-index pure fused silica core/F-doped fused silica cladding but with an aluminum coating rated to temperatures of 385°C .
- 3) Optran WF200/220P.
This is a low OH step-index silica/silica fiber with a polyimide jacket of $240\text{ }\mu\text{m}$.

Figure 10: Properties of Fibers in Toossi and Modarress Experiment

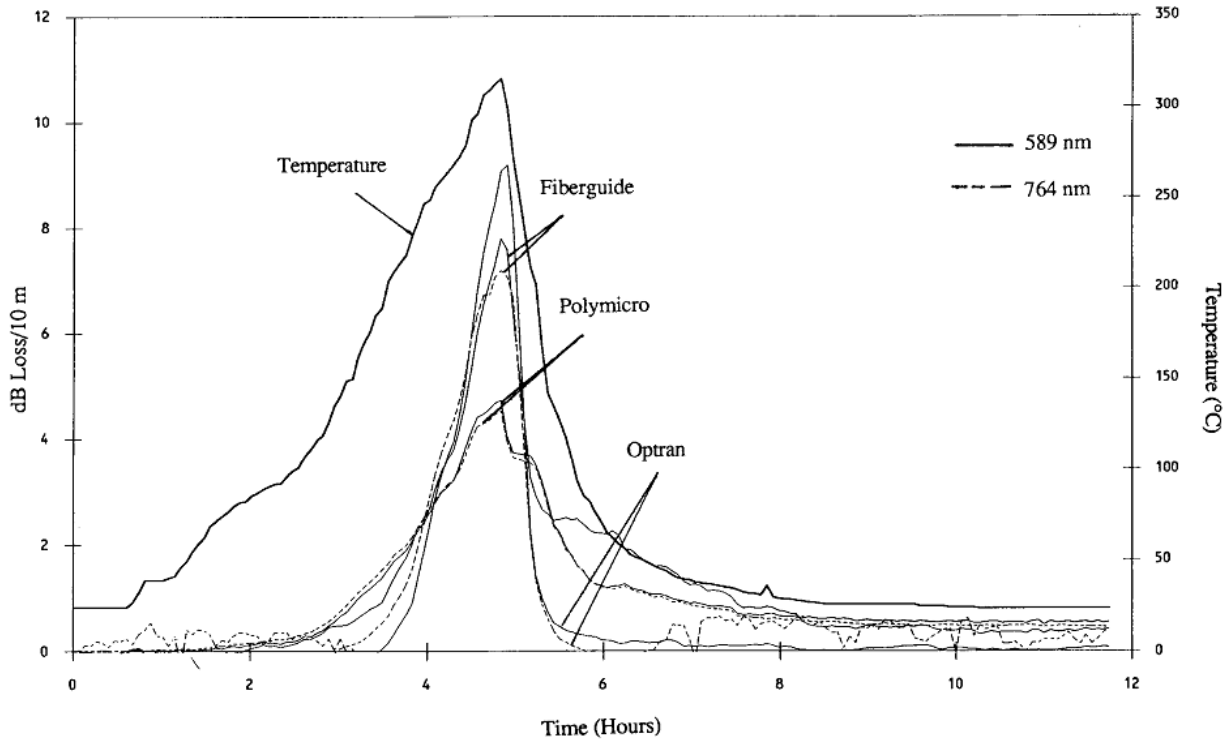


Figure 11: Effect of Temperature on Fiber Degradation, Toossi and Moddarress Experiment

In this experiment the temperature effects on the fibers are significant, with large losses above around 200 °C. The authors do not have a complete explanation of this effect, attributing it to the possibility of jacket or cladding damage. Later in this report an attempt will be made to recreate this experiment, and understand the effects of temperature on silica fibers.

Due to the three factors mentioned above, the upper limit on the use of silica fibers is approximately 900 °C (Wang, Zhu and Pickerell). This limitation results in the need for another material for higher temperature applications, and sapphire fibers, with a melting point of greater than 2000 °C presents great promise in filling this need. In various studies, sapphire fiber based

temperature sensors have been operated at temperatures from 1500 °C to 1600 °C, and the main limitation on their operation has simply been the inability to accurately generate high temperatures for testing. Wang, Zhu and Pickerell expect that the sensors could operate at temperatures even approaching the melting point of sapphire. Zhu and Huang discuss a study in which a sapphire-based EFPI sensor was tested to 1600 °C with excellent reproducibility and accuracy, and again they expect that the sensor could be used at temperatures near the melting point of the sapphire. They also suggest that the use of alternative types of crystal could be used to extend the operating range even higher (Zhu and Huang).

In addition to sapphire based EFPI sensors, recent work has shown the feasibility of Fiber Bragg Gratings in sapphire fibers. Grobncic and Mihailov reported in 2004 that they had successfully created Bragg gratings in sapphire, and tested them up to 1500 °C (Grobncic and Mihailov). The gratings, interrogated using a tunable laser with a range of 1460-1580 nm, showed no sign of degradation at temperatures up to 1500 °C, and again as with testing on EFPI sensors are expected by the author to survive temperatures up to 2000 °C.

2.3 Summary

The nature of fiber optics and optical sensors lends them to applications in harsh environments. Reactor environments present multiple challenges that must be met by any instrumentation that is to survive the harsh conditions, and optical sensors have shown promise in their ability to withstand these conditions. Both EFPI sensors and Fiber Bragg Gratings present favorable characteristics for such environments, with FBG sensors providing the greatest benefit due to their ability to be multiplexed. The ability to apply these sensors depends on the

survivability of the fiber, and research has shown the ability of silica fibers to withstand relatively high temperatures. However, this requires the use of specialized coatings to maintain the mechanical strength of the fibers, and they are still vulnerable to crystallization of the fiber, thermal diffusion of the dopant, and softening of the glass, which all contribute to losses in the fiber at high temperatures. This effectively limits the operating range of silica fibers to 900 °C. For higher temperature applications, sapphire fibers have proven to be effective at temperatures up to 1600 °C, and are expected to perform at temperatures approaching their melting point, greater than 2000 °C.

CHAPTER 3: METHODS

3.1 High Temperature Furnace Design

The first priority of this project was to design a furnace capable of testing single-crystal sapphire fibers in a nuclear reactor environment, and a significant amount of work was done to overcome some of the key challenges to designing such a furnace. The furnace had a variety of design constraints that needed to be satisfied. The first constraint was in the size and shape of the furnace, as it had to fit in a seven inch dry tube at the OSURR, and be capable of accommodating the sapphire fiber. The next constraint was that the furnace must reach internal temperatures in excess of 1500°C, while limiting the external temperature such that the surrounding water in the reactor pool stays safely below boiling temperature. The third constraint was that the furnace materials must be compatible with the reactor, both in terms of avoiding any significant change in reactivity, and limiting activation as much as possible. A fourth constraint is that the entire furnace must be able to be easily raised and lowered into the reactor, without risk of any part of the furnace, or fiber, breaking and remaining in the dry tube upon removal of the device. Another key consideration is safety, and the furnace design requires that the control system include multiple redundancies to ensure that the furnace is operated within strict pre-defined conditions, and is shut down safely if any aberration occurs.

3.1.1 Sapphire Fiber Specification

As the entire design of the furnace depends on the fibers available for testing, the first consideration in the design was to specify the single-crystal sapphire fibers that would be tested. Commercial sapphire fibers, from MicroMaterials Inc., were available in-stock in lengths of 1 m, with a diameter of 125 μm or 100 μm . Other custom sizes are available, as shown in Table 1, below, but for this project fibers of 1 m in length, and 125 μm in diameter were chosen since they were available in stock.

Table 1: Available Sapphire Fibers, MicroMaterials Inc.

Sapphire Fiber Selection Chart	
Diameter	Max. Length
305 - 500 μm	50 cm
205 - 300 μm	100 cm
100 - 200 μm	200 cm
75 - 95 μm	100 cm
	*100 μm fibers with 100 cm length (SF100-100) and 125 μm fibers with 100 cm length (SF125-100) are stock items.

In testing silica fibers, it is common to test much longer lengths of fiber. ASTM Standard E 1614-94 specifies that for testing of irradiation effects in fiber optic cables, lengths of 50 ± 5 meters should be used (ASTM). In the design of the silica-fiber furnace our lab has attempted to accommodate this by designing a heater in which long fibers can be coiled many times. This introduces the constraint of minimum bend radius of the fiber to the heater design. For 125 μm

sapphire fibers, the minimum physical bend radius is 2 cm. In addition to the physical bend radius, it is important to consider limits placed on the bend radius due to optical properties of the fiber. Optical losses are specified by the manufacturer as 3% for a 3 cm diameter loop in 100 μm fibers. For the purposes of designing the high temperature furnace it was determined that although the minimum bend radius of the fibers would allow multiple loops to be tested, much like in the silica fiber furnace, other constraints on the design favored testing a single length of fiber. Because the fiber is only 1 meter in length, any attempt to loop the fiber within the furnace would gain minimal benefits at the cost of significant complexity. It is also possible that two lengths of fiber could be tested, by threading the fiber through the furnace from top to bottom, looping it around at the end, and threading it back through the furnace in the opposite direction. This would increase the amount of fiber in the heated length of the furnace, as well as simplify the setup needed to connect the sapphire fiber to the optical equipment via silica fibers.

3.1.2 Heater Specifications

The most important component of the furnace is the heater, as it is crucial to meeting each of the design constraints listed above. The first constraint that must be addressed is the size of the heater, and it depends primarily on two factors. The first is the diameter of the dry tube, and the second is the orientation of the sapphire fibers. In addition, considerations must be made for temperature, as the thickness of the insulation determines the ability to maintain the outside temperature of the furnace at acceptable levels. As discussed above, it was decided that due to the nature of the sapphire fibers available, it would be most logical to test a single length of fiber, rather than attempting to increase the irradiated/heated length by looping the fiber within the

heater. This design decision led to the choice of a cylindrical tube heater, as such a heater would accommodate a single length of fiber quite easily, and allow us to maximize the thickness of insulation. Figure 12, below, is a schematic of the heater chosen (MHI).

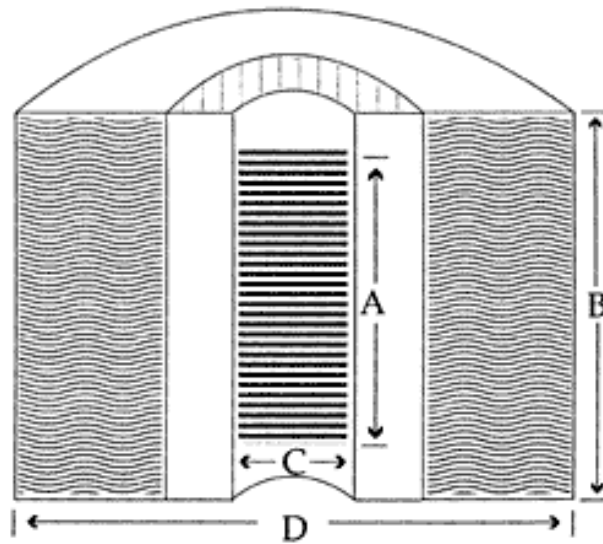


Figure 12: Schematic of Tube Furnace from MHI

This type of heater was chosen because the decision to test a single length of fiber allowed us to minimize the inner diameter, C, while choosing the maximum outer diameter, D, that would be compatible with the size of the dry tube, thus maximizing the thickness of the insulation. The final dimensions of this heater are 12" heated length, A, 15" overall length, B, 1" inner-diameter C, and 6.5" outer diameter, D. Figure 13, below, shows an actual example of the heater. This particular model, the Inline Robust Radiator, was chosen because the leads extend from the top of the furnace, rather than the side, and this is the only option compatible with the geometry of the experimental facility. The metal bands around the circumference of the heater will be

removed due to activation concerns, and the insulation will be held in place by the aluminum structure discussed later in this section.

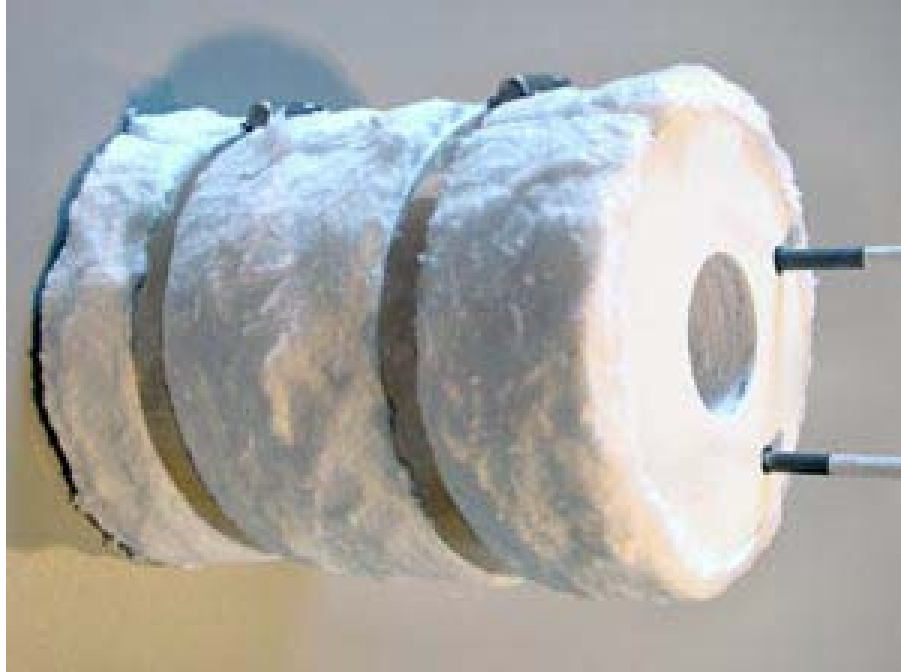


Figure 13: Example Robust Radiator Heater from MHI

3.1.3 Heater Instrumentation

Another important consideration in the design was the choice of instrumentation to measure the temperature of the heater. It was determined that the most practical option would be to use a thermocouple, and the appropriate thermocouple type for the needed temperature range was a Type B thermocouple. Type B thermocouples use Platinum-Rhodium thermoelements, one with 30% rhodium, and the other with 6% rhodium. These thermocouples are appropriate for continuous use at temperatures between 870 and 1700°C, and under corresponding conditions

they show less grain growth and less drift in calibration than Types R and S thermocouples, also of the platinum-rhodium type (ASTM International). The difficulty with the use of thermocouples, or any other means of measuring temperature, is the inability for our lab to calibrate such devices at the high range of temperatures they will be operating at. However, it was decided that the thermocouple should be initially calibrated by the manufacturer, and the relatively short operating time of the thermocouple, as compared to continuous usage in an industrial setting, will likely allow it to remain accurate enough for our purposes. It is also much cheaper to replace the thermocouple in the case that it does lose accuracy than to pay to have it recalibrated, so this option seems to be the best for our initial trials. Laboratory testing once the furnace has been constructed will help to reveal any problems with this strategy before introducing the experiment to the nuclear reactor environment.

3.1.4 Furnace Structure

The next important consideration in the design of the furnace was the issue of containing the heater, ceramic end caps, and other equipment in a structurally sound package that can be easily lowered into and raised out of the dry tube at the OSURR, as well as set up on a lab bench in Scott Lab for testing. Important considerations include the strength of the material chosen, but also concerns with activation of the material. Issues with activation must be reduced by choosing a balance between strength of the material and its propensity to activate, as well as by reducing the overall amount of material introduced to the reactor, because even small proportions of impurities within a material can make a sizable difference. The initial CAD drawings for the design for the furnace can be seen in Figure 14, below.

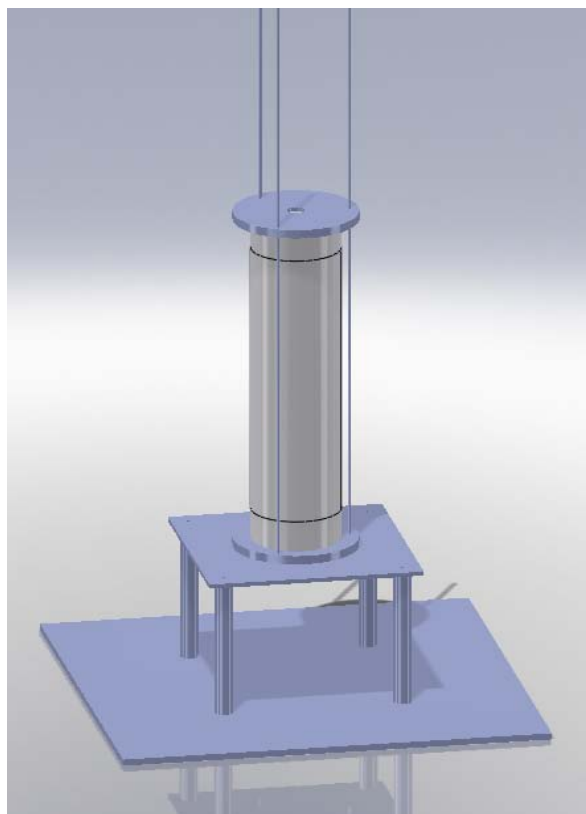


Figure 14: Initial CAD design for High Temperature Furnace

Initially aluminum 6061 was chosen for the structural material, as it was believed to be the best suited for balancing concerns about activation, and material strength. The light gray cylinder is the heater itself, and the two end caps. The light blue material is all aluminum 6061, with thin 1/4" circular plates at the top and bottom, connected by #10-24 aluminum all-threads. The base, including a 18"x18"x3/8" base plate, with a 12"x12"x1/4" plate supported by 4 12"x1" diameter legs were all constructed using aluminum 6061 as well, though these parts will not be introduced to the reactor. This was determined to be an appropriate choice so that the base materials can be repurposed for other experiments in the reactor once the base is no longer

needed. This design was used in the construction of the prototype heater which will be discussed further in the next section.

Some important adjustments have been made to the final design since construction began on the prototype. The first major change is that the aluminum alloy will be changed to aluminum 3003 for all plate materials. This is due to further calculations concerning the activation products of these two alloys, performed by Chris Petrie, which has indicated that although 3003 is not as strong as 6061, its superior activation characteristics make it a much safer and more practical choice than 6061. Another important change will be replacing the use of all-threads with more rigid aluminum bars. This change will increase strength and rigidity of the structure. These parts will likely remain aluminum 6061, due to the increased importance of strength in this particular part of the design.

In addition, plates were added above and below the furnace, both to give the overall structure additional stability and prevent the tendency for the plates to torque around the axis of the heater due to the flexibility of the aluminum all-threads. This will also be helped by using aluminum bars rather than all-threads, as described above. These plates also serve the purpose of helping to locate the fibers, as well as thermocouple wires, that will be connected to the furnace during operation. Another important issue which remains to be remedied is the method by which the thermocouple will be inserted into the heater. A hole has been drilled in the side of the heater, and this will be sufficient to allow the thermocouple to be inserted for testing in the lab. For testing in the reactor, however, the sensor will need to be inserted in another manner due to space limitations within the dry tube.

3.1.5 Control System

Further design challenges were presented by the need for a reliable control system, which can safely shut down the experiment under any unusual conditions and avoid any dangerous conditions during testing in the lab, and more importantly in the reactor. This was not of particular concern to this project, as the control system that will be used for the high temperature furnace will be shared with the lower temperature silica fiber testing furnace that is being designed simultaneously by the lab. David Hawn has done extensive work on this part of the project, and construction on the control system should begin by the end of this quarter, with initial testing to follow soon after.

3.2 Furnace Prototype

Due to the nature of the high temperature furnace, both its high cost and long planning period, it was prudent to build a prototype furnace for the dual purposes of helping to overcome future design issues before facing them during construction of the final furnace, and for allowing preliminary data to be collected in a timely fashion. A prototype of the heater was constructed in Scott Lab, conforming as closely as possible to the design of the high temperature furnace using relatively inexpensive materials, and when possible, equipment already available in the lab. In this section, the design of the heater, as well as some issues faced during construction, will be described.

3.2.1 Prototype Heater

Just as the high temperature furnace was based around the specified heater, the choice of a heater was one of the more important factors in the design of the prototype furnace. The heater used was chosen simply based on availability, as a tube furnace with control system were already available in the lab. The furnace, by Watlow, was very similar in design, but significantly smaller than the heater specified for the high temperature furnace. Both are electric heaters, and use a coil design, with ceramic insulation. The inside diameter of the prototype heater was 1", but the outside diameter only 3". The length was 12", with the entire length being heated, unlike the high temperature heater. The heater's maximum temperature was 1093°C, significantly lower than the maximum temperature of the high temperature heater. This temperature limit was the most important factor in influencing the remainder of the design decisions regarding the prototype. Because we plan on testing the sapphire fibers at temperatures exceeding 1500°C, it was decided that the prototype would only be used to test silica fibers. This way, the expensive sapphire fibers can be saved for the high temperature furnace, and we can be sure that they all start from the same baseline, rather than causing some change in the fibers at lower temperatures that will make comparison of future results more difficult.

3.2.2 Prototype Heater Controller

Temperature control was accomplished using a heater controller that had previously been used with the heater. The Digi-Sense controller, from Cole-Parmer Instrument Company, can be

seen in Figure 15, below. No manual was available for the furnace in the lab, or online. The controller does not appear to be sold any more, as newer models with automatic calibration and digital controls are readily available.



Figure 15: Digi-Sense Temperature Controller

The controller uses a type K thermocouple to measure the temperature. The heater is relatively easy to control, as the set-point temperature is controlled using a simple knob, and the controller automatically adjusts to new temperature settings. Due to the lack of manual, however, the ability to finely tune the temperature was limited. In the top-right of the front panel of the controller are screw adjusters for the variables “Over Temp,” “Prop. Range,” and “Prop. Offset.” Through trial-and-error it was unable to be determined how to accurately calibrate the heater using these settings. Instead the temperature setting must be very slowly adjusted upwards, as the heater is prone to overshooting. In addition, the final set-point value chosen should be approximately 10°F lower than the intended value, as the heater has a significant steady-state error.

3.2.3 Prototype Furnace Instrumentation

Instrumenting the furnace turned out to be the greatest challenge of building the prototype. The controller requires one type K thermocouple to measure the temperature of the heater. In addition, a second thermocouple was used to provide confirmation of the temperature in case the control thermocouple were to fail. This second thermocouple was monitored using a simple Omega Thermometer, as shown in Figure 16, below.



Figure 16: Omega Thermometer for Backup Thermocouple

The confined space inside the heater, with its 1" inner diameter, and the high temperatures reached during testing, made it very difficult to correctly locate the thermocouples. It was important that they be located as close to the center of the heater (axially) as possible, as this would be the location of the fiber. At the same time, it was important that room still be left for the fiber. One of the first attempts at locating the thermocouples used ceramic insulators and copper wire. A long section of ceramic was braced by two shorter (approximately 1") sections, such that it could be inserted into the heater, and the cross-braces would maintain spacing from

the walls of the heater. Copper wire was used to attach the cross braces, as well as attach thermocouples to the insulator. Figure 17, below, shows one attempt at this setup.

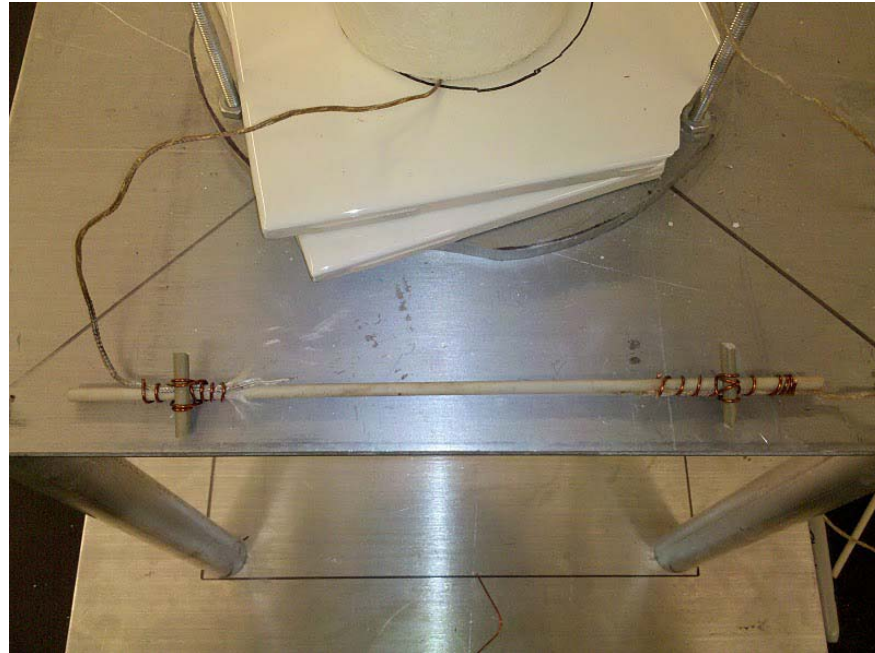
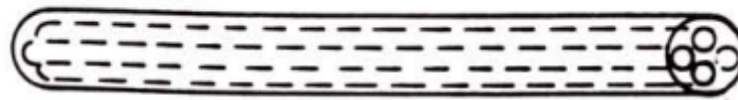


Figure 17: Initial Attempt at Locating Thermocouples

This design had a variety of flaws. The first was the inability of the materials to withstand the high temperature environment. The copper wire available for this use had a coating that would burn off, leaving the windings loose and causing the braces to fall off. In addition, the thermocouples themselves could not withstand the heat, as the insulation would become discolored, and then slowly disintegrate away over the course of testing. The discoloration can be observed in Figure 17, above, particularly in the thermocouple on the left. The insulation of this thermocouple has turned completely white, and will soon completely disintegrate. The final issue with this design, and possibly the most important, is that every time

the experiment was set up again, the thermocouples and ceramic insulators would have to be removed and re-inserted, which caused a number of issues. The first is that inconsistent temperatures would result due to varying placement of thermocouples from experiment to experiment. The second is that the stress of trying to reposition the thermocouples would lead to further damage to their insulation, and in one case resulted in a short, in which the control thermocouple essentially was measuring the temperature at a location other than the welded junction. This becomes dangerous because the thermocouple becomes less responsive, due to the larger thermal mass that must be heated at the location of the short. Because the heater controller already had a tendency to overshoot, this would result in temperatures much higher than intended, as the controller would continue heating the furnace long after the correct temperature had been reached.

A variety of other possible designs were attempted before the final design was finally complete. In the final design, the ceramic insulators were used once again, but this time they were used as they were originally intended, with the thermocouple wires inserted through the bore holes, thereby preventing the issue of shorts due to disintegrating insulation. The ceramic insulators used were of the round four bore type, as pictured in Figure 18, below (ASTM International).



Round Four Bore Insulator

Figure 18: Four Bore Ceramic Insulator

The problem of locating the thermocouples was solved using a steel all-thread that was located in the center of the heater by locating it in the center-holes of the aluminum plates and ceramic tiles. The insulators were affixed to the all-thread using uncoated copper wire which was threaded through one of the bore holes, and wound around the all-thread at either end. Two ceramic insulators were used, each with one thermocouple, and they were arranged such that both thermocouple junctions would meet at the center of the furnace. Each ceramic insulator is 6" long, such that they meet in the middle, and extend to either end of the furnace, protecting as well as locating both the thermocouples and the fiber that is being heated. Figure 19, below, shows a close-up of the way the ceramic insulators were attached to the all-thread, and Figure 20 shows the location of the sensors with the heater removed, to show the relative location of the sensors in the furnace. Of note in Figure 20 is the fact that the copper wires, as well as the steel all-thread, have blackened, as this picture was taken after testing the furnace at temperatures exceeding 750 °C. This is one weakness of the system, as the copper wires loosen and allow the ceramic insulators to shift their position over time. This means that in order to thread the fiber through without disassembling the system, as described later in this chapter, the system must still be periodically disassembled and re-adjusted, resulting in potential damage to various

components, including further weakening of thermocouple wires, particularly at the ends of the ceramic insulators where they exit the furnace.



Figure 19: Attaching Ceramic Insulators to Steel All-thread

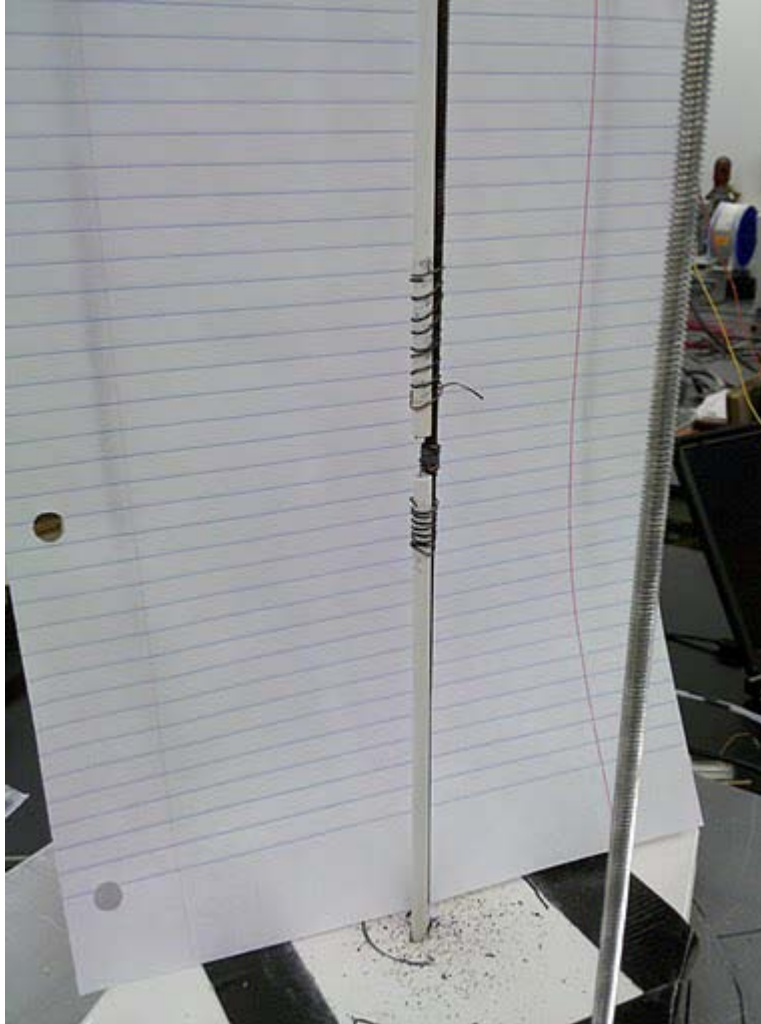


Figure 20: Final Layout of Thermocouples in Prototype Design

Another important issue that was also solved using this design was the issue of continually taking apart and re-assembling the furnace each time a fiber is loaded. The ability of the thermocouples to operate continuously and remain precisely located removed the need to constantly adjust them. Next, it was determined that the fiber could actually be threaded through the final hole in the ceramic insulators. This ensured a consistent location for the fiber, and allowing it to be easily threaded through the device without removing the heater every time.

This is important because the device is not set up to be easily adjustable by one person. Further, it is important because the actual heater will one day have been activated in the reactor, and the easier it is to unload and load a fiber the safer the experiment will be. It is important that this be taken into consideration in the final design.

3.2.4 Prototype Furnace Structure

The next design decision was how to construct the aluminum frame. Despite the smaller size of the available heater, it was determined that the full size frame would be constructed, according to the initial design. This would not only more closely follow the original design, allowing any design issues to be solved, but it would also potentially be adapted to the final furnace without the need to re-machine the parts in the future. As discussed above, the construction of the frame revealed some important issues that required changes to be made to the final design. The primary difference will be the change to the design of the plates that hold together the furnace, and the aluminum bars which will replace the all-threads. The CAD drawings for each individual part of the structure can be found in Appendix A, in addition to assembly drawings showing the overall design.

3.2.5 Prototype Furnace Insulation

For the design of the prototype it was determined that purchasing ceramic end-caps for the heater would not be justified for this low-temperature application. It was instead decided that simple ceramic tiles would be tested to determine their ability to insulate the system. A

photograph of these tiles can be seen in Figure 21 below. A hole was drilled in the middle of the tiles using a ceramic drill bit, and they were later cut down to a small enough size to fit in place.



Figure 21: Ceramic Tiles Used as End-Caps for Prototype Heater

Initial testing of the heater, before the addition of the end-caps, showed that using the heater controller, discussed above, it was very difficult to maintain the desired temperature, as large fluctuations in temperature would occur. These fluctuations would have made it nearly impossible to control the heater, but with the addition of these ceramic tiles, the fluctuations were almost completely eliminated. Two tiles were added above, and two below the furnace and in testing as high as 750 ° C the tiles have had no problem withstanding the heat. Aside from some slight discolorations, particularly on the tile immediately in contact with the top of the furnace, there have been no noticeable changes in the tiles, and they continue to perform adequately. It has been decided that there is no further need to modify or improve upon this simple solution.

3.2.6 Prototype Optical Equipment

The final component of the prototype was the optical equipment. A light source and spectrometer, both from Ocean Optics, were used to interrogate the fibers, and software called Logger Pro was used to collect the data. The light source, model number LS-1 is a tungsten halogen light source, with a range of 360-2500 nm. It has an SMA 905 connector. Manufacturer's specifications for the light source can be found in Appendix C. During testing, the voltage regulator on the device failed. It was replaced using a newer chip, as the part was obsolete, and the design was improved by adding a capacitor specified by the voltage regulator manufacturer. This should improve the reliability of the device in the future.

The spectrometer used, also from Ocean Optics, was the USB 2000 model. This device also has an SMA 905 connector, and connects to a computer via USB for real-time data collection. The range of the device is 200-1100 nm, and the full manufacturer's specifications can be seen in Appendix D. Thus, the overall range available for testing using this particular setup is 360-1100 nm. This is sufficient to gain insight into the operation of silica fibers, but it is important that for future fiber testing the range be expanded above 1100 nm. Communication bands typically range from 1200-1700 nm.

3.2.7 Prototype Fiber Connectors

In order to connect the fibers to the optical equipment, Bullet Bare Fiber Adapters were purchased from Fiber Plus International. The adapters purchased consist of an aluminum fiber holder, with a steel SMA 905 connector module that allows the fibers to be connected to the

optical equipment described above. A photograph of one of these connectors can be seen in Figure 22, below.



Figure 22: Bullet Bare Fiber Adapter

The connector modules are interchangeable, such that they could be replaced in the future if an alternative form of connectors were required for new optical equipment. The particular parts purchased are custom adapters for 250 μm fiber, with low-density padding, which is used to help prevent damage to the fibers. The adapters are ideal for the purposes of testing at Scott Lab, as they allow fibers to be very quickly and easily attached to the optical equipment, without permanent change to the fibers themselves or any need for special equipment. They also have the potential to be used in testing at the reactor, as the bulk of the material is aluminum, with the steel connector modules having the ability to be removed and replaced as needed. Though this is not the ideal solution for this application, it is important to consider removable connectors such as these, in particular for the testing of the very expensive sapphire fibers.

3.3 Silica Fiber Testing Procedures

Once the prototype construction was complete, the next step was to begin testing of silica fibers. This served the dual purpose of giving additional practice handling the furnace setup, as well as the fibers, and it also allowed us to begin looking in detail at the performance of the silica fibers in a high temperature environment.

3.3.1 General Fiber Testing Procedures

In order to test each silica fiber, a length of fiber of approximately 2 m was chosen, and the ends were polished using the fiber polishing kit in the lab. The fiber was then carefully threaded into the furnace, through the holes in the aluminum plate at the top, the ceramic tiles, and into the ceramic insulator described earlier. At the middle of the heater the fiber exits one ceramic insulator briefly before entering the second ceramic insulator, and proceeds out of the furnace through the ceramic tiles and aluminum plate at the bottom. Threading the fiber through the furnace in this way, although much easier than previous attempts in which the heater was removed and replaced to load the fiber, is still difficult and fairly often results in breaking of the fiber. If the fiber breaks, it is simply re-threaded through, and the broken end is re-polished. Once the fiber has been threaded through the furnace, the ends are connected to the spectrometer and light source using the Bullet Bare Fiber Adapters as described above.

3.3.2 Repeating Previous Experiment by Toossi and Modarress

The first testing that was done was to try to recreate as closely as possible the results of the 1991 study by Toossi and Modarress, as described in the “Heating Silica Fibers” section of

Chapter 1 of this thesis. The study performed a variety of tests on the effects of both temperature and radiation on silica fibers, but we are concerned here simply with the temperature effects. Figure 11, in the above description, shows the results of a test in which silica fibers of three types were heated to approximately 325°C over the course of 5 hours, and then cooled back to room temperature. The same procedure was used as described in this previous study, and the same wavelengths were monitored, with four additional wavelengths monitored as well. The biggest differences between the two experiments were the fibers used, and the length of the fibers being tested. In the previous study 10 m lengths of three different types of silica fiber were heated, but in this experiment only 12 inches of fiber are heated. The results of this initial test can be seen in Figure 23, and Figure 24, with the second figure showing the additional wavelengths.

3.3.3 Prototype Testing at Increasing Temperatures

Because little change in the attenuation of the fibers was observed in the first test, it was decided that the fibers would be tested at higher temperature. In the second experiment the temperature would continue to be raised in an attempt to cause a more measurable change in the output. The temperature was stepped up to 750 °C, which was determined to be the maximum safe operating temperature of the prototype heater. The results of this test can also be seen in Figure 25, and Figure 26 below.

After conducting this test and determining that heating the fibers to temperatures greater than 500 °C was necessary, a final test was conducted in an attempt to further verify the results obtained. In this final test, the fibers were heated to greater 750 °C once again, though over a

shorter time than in the previous test, and with a one hour dwell in the temperature at 750 °C. The results of this final test can be seen in Figure 27 in the Results section, below.

3.4 Summary

The high temperature furnace, which will be used to test sapphire fibers at the OSURR, has been designed and the majority of the parts have been specified and ordered. It meets all of the important design criteria as closely as possible, and prototype testing has helped to support some important design considerations, such as the choice of a tube furnace, the need for a hole to be drilled in the side for instrumentation purposes, and the stability of the aluminum frame. The prototype testing has been successful, both in that it has helped to verify the overall design and helped to bring to light the challenges that will be faced in constructing the high temperature furnace, and in that it has allowed us to collect important data on silica fibers. The testing of silica fibers, though initially unreliable without good fiber connectors, has been remedied, and has shown the fibers to be capable of withstanding very high temperatures.

CHAPTER 4: RESULTS

4.1 Prototype Furnace Silica Fiber Testing

As described in the Methods section above, various tests on silica fibers were conducted using the prototype furnace that was constructed. The first of these attempted to follow the procedure used in the previous study by Toossi and Modarress. Later experiments raised the temperature the fibers were heated to, and added the use of Bullet Bare Fiber Adapters, which greatly improved the results.

4.1.1 Repeating Previous Experiment

Figure 23, below, shows the results of the first test described in Section 3.3.2, which was again intended to replicate the results of testing by Toossi and Modarress. Six wavelengths were sampled in this test rather than two. Figure 23 shows only the wavelengths used in previous testing, for comparison, but Figure 24, below, shows the same graph with all six wavelengths included.

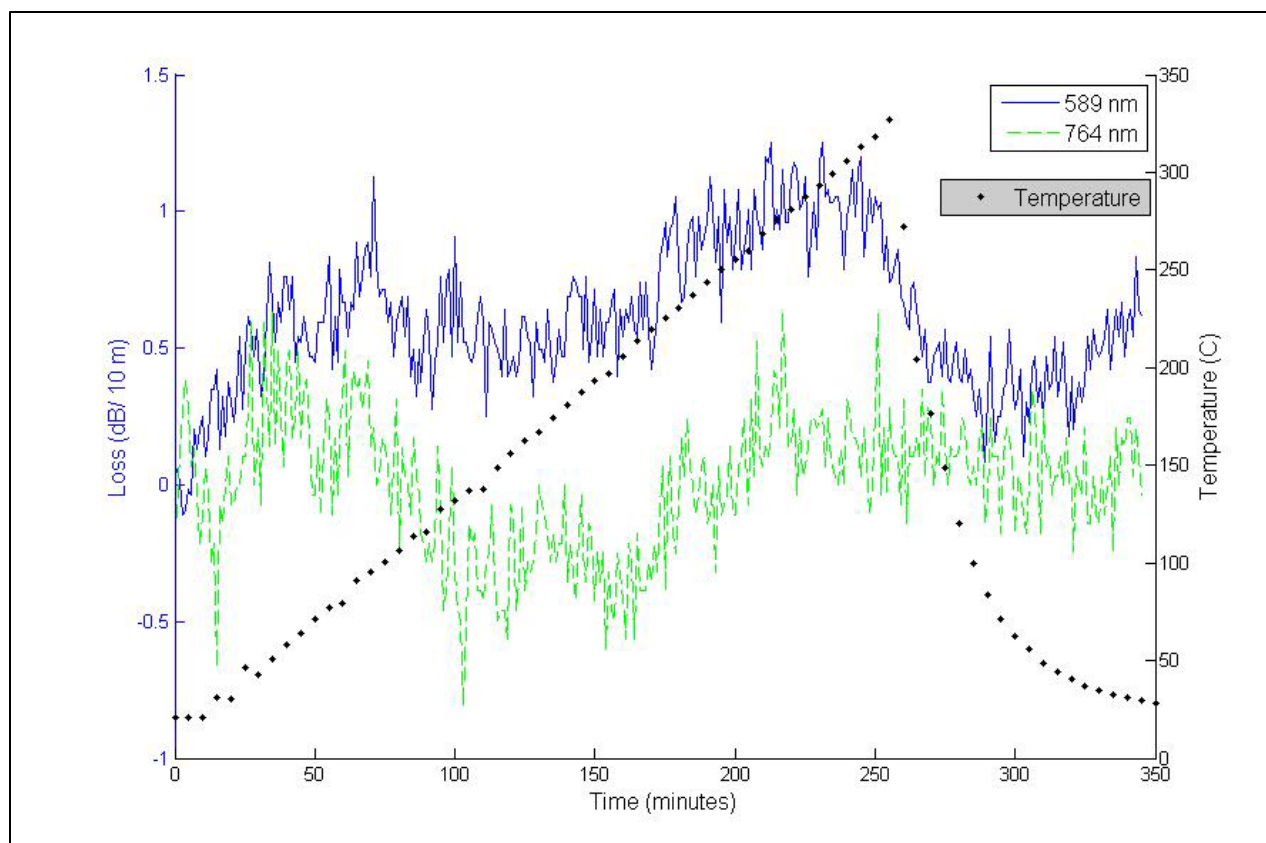


Figure 23: Prototype Testing, 325 °C

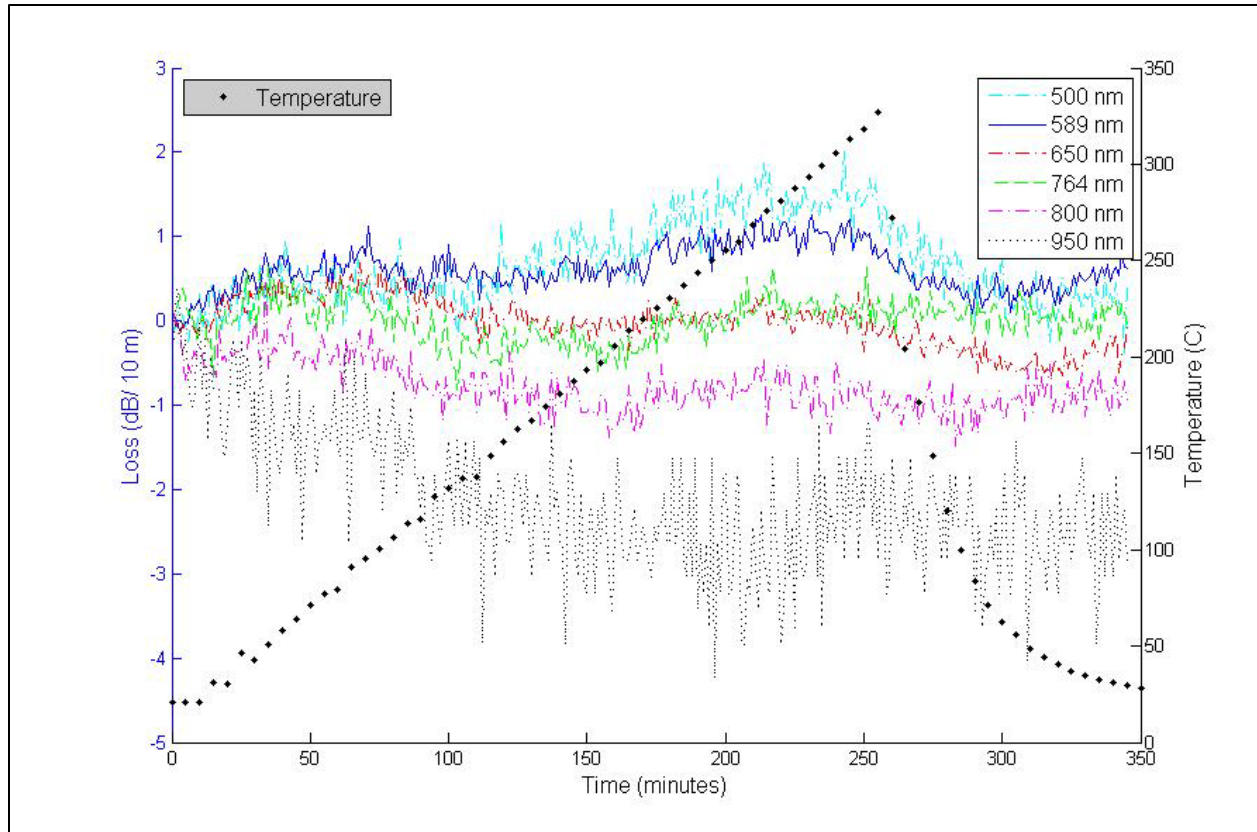


Figure 24: Prototype Testing, 325 °C, Additional Wavelengths

4.1.2 Higher Temperature Testing, With Connectors

Figure 25, below, shows the results of the second test described in section 3.3.3, and the fibers were tested to the maximum operating temperature of the prototype furnace, 750 °C. Figure 26, below, shows the same graph with additional wavelengths added in. A final test was conducted in which the temperature was more quickly raised to 750 °C and remained at this temperature for one hour before returning to room temperature. This can be seen in Figure 27, below.

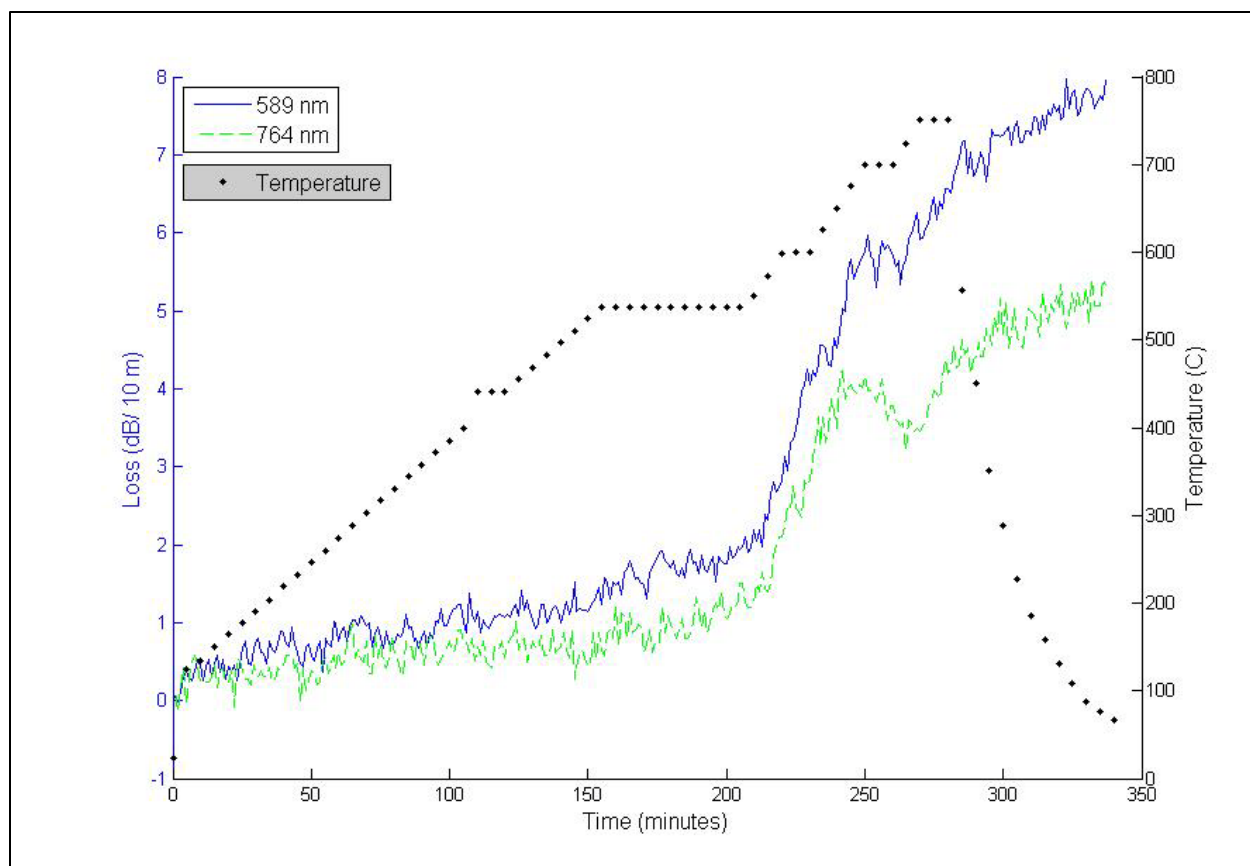


Figure 25: Prototype Testing, 750 °C

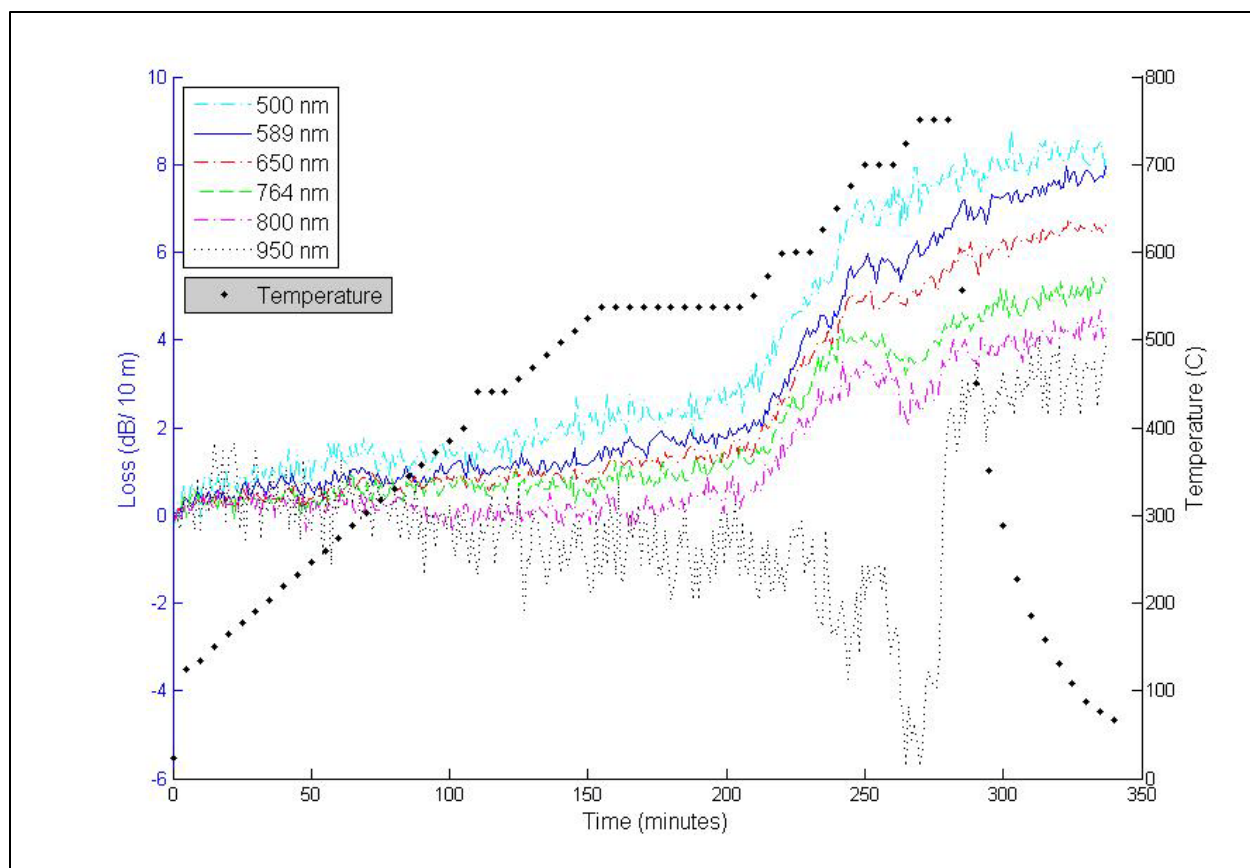


Figure 26: Prototype Testing, 750 °C, Additional Wavelengths

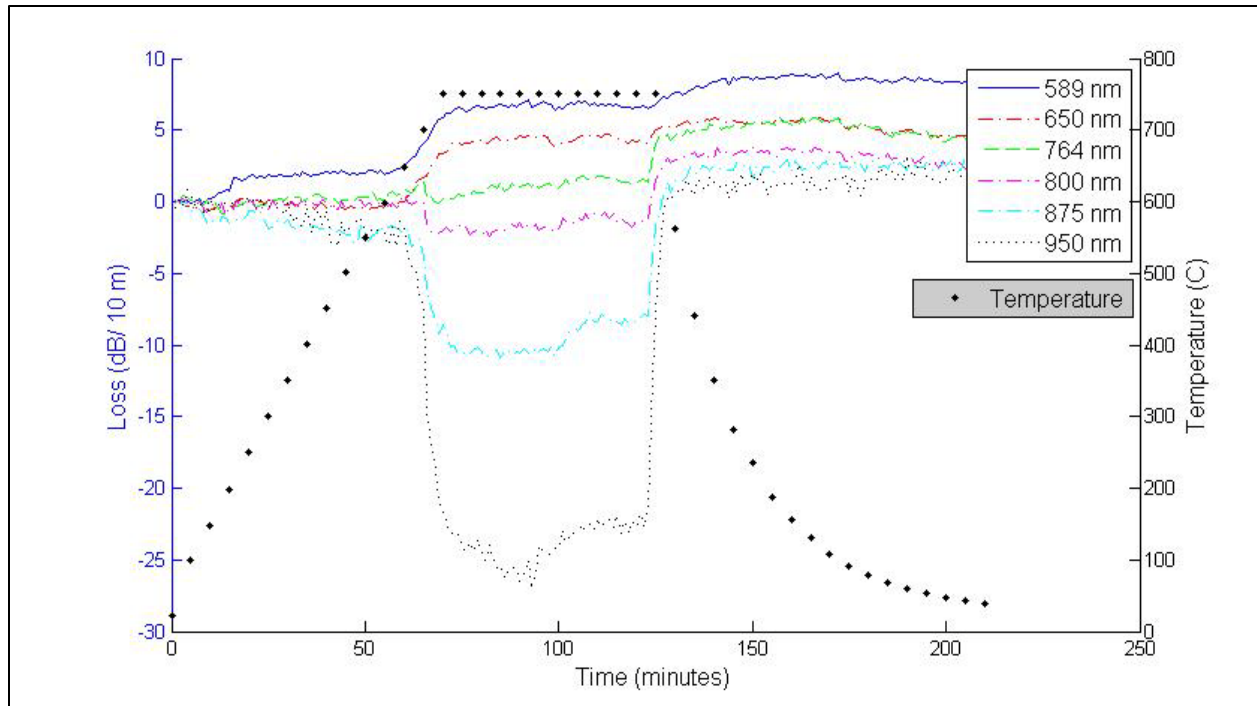


Figure 27: Prototype Testing, 750 °C Prolonged Test

4.2 Physical Damage to Fibers

As described in section 3.3.3, above, it is important to consider the physical damage to silica fibers at high temperatures in addition to their optical properties.

Figure 28, below, shows the entire heated length of fiber. On the far ends of the picture are unheated sections of fiber, and the color transitions to a dark brown, then black, before becoming clear as the fiber goes toward the center of the heater. Figure 29, below, shows a close up of one end of the fiber, giving a clearer picture of this transition.

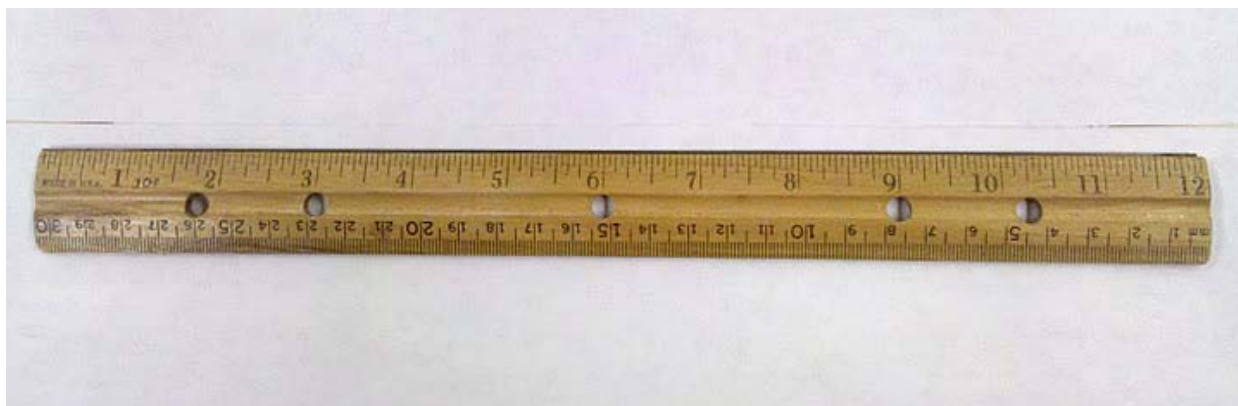


Figure 28: Physical Damage to Fiber, Prototype Heater Testing at 750 °C



Figure 29: Physical Damage to Fiber, Prototype Heater Testing at 750 °C, Close-Up

CHAPTER 5: ANALYSIS

Preliminary testing of the silica fibers using the prototype heater has led to some interesting results which will be useful for future work on this project. The effects of high temperature on the particular silica fibers being tested in the lab are beginning to be better understood, though much more testing and further literature review will be necessary to understand and break down the various different factors that are affecting their behavior. Preliminary testing has shown that the fibers do much better at temperatures below 500 °C than the fibers tested by Toossi and Modarress, but that they begin to be significantly affected by temperature as it reaches and exceeds around 600 °C. In addition, lab testing has shown the severity of the embrittlement of the fibers due to the destruction of the coating at high temperatures, and further justified the need for higher temperature materials.

5.1 Optical Performance of Silica Fibers

5.1.1 Optical Testing

The first test, as described in the Methods section above, attempted to replicate the results of the Toossi and Modarress experiment at 320 °C. The results of this test can be seen in Figure 23 and Figure 24. In this test it appears that what was surmised in the previous testing, that temperatures this low had very little effect on the fiber, seem to be true. In this case six wavelengths were tested, and it appears that for the most part the losses in the fibers were minimal, ranging from -1 to 1 dB/10 m. The notable exception is at 950 nm, where the losses

actually reach -3 dB/10 m. Overall the variation in the fiber seems small, and it is difficult to attach any significance to these results without further testing.

Next it was decided to attempt to heat the fibers to a temperature at which a more noticeable change in attenuation would be noticed. Initially it was decided to heat the fibers to 550 °C. Midway through the test, as it was observed that very little change in the intensity of light had occurred during the dwell period at 550 °C, it was decided that the test would be extended and the fiber would be heated to the maximum temperature of the furnace, 750 °C. As the fibers continued to be heated, significant attenuation began to occur. Starting with the first increase over 550 °C the attenuation in the fiber closely tracked the increase in temperature, continuing all the way to the maximum temperature at 750 °C. In addition, the fibers did not improve after they cooled, with the attenuation actually continuing to increase slightly during the cooling time. Again the 950 nm wavelength is the notable exception, with improvements in the losses occurring at around 700 °C, and then disappearing as the fiber was cooled. The 764 nm and 800 nm wavelengths show a similar, though much less pronounced, effect at this temperature, indicating that further attention may be justified at this temperature. Further testing will be done to determine what might be causing this effect.

Another interesting result of this test is that as the wavelength increases, the losses in the fiber at high temperature become less severe. This difference is large enough that the final losses in the fiber, shown in Figure 26, indicate that at wavelengths of 500 and 589 nm the losses are approximately twice the losses at wavelengths of 800 and 950 nm, around 8 dB/10 m vs. 4 dB/10 m respectively. This is encouraging because these higher wavelengths are of more interest for

our applications, and future testing will actually be conducted at even higher wavelengths once the appropriate optical equipment is purchased. The current light source and spectrometer combination results in a significantly lower photon count at 950 nm, which leaves the output more susceptible to random variations in output, and could explain some of the unexpected behavior at this wavelength.

In order to better understand this result, one final test was conducted in which the fibers were heated to 750 °C once again, but remained at this temperature for an hour. This helped to determine whether the effects that were noticed at higher wavelengths were due to experimental error, or another factor. The result of this experiment can be seen in Figure 27, above. The fibers again are very resilient up to around 600 °C, when losses begin to appear. Here the effect that was noticed at 950 nm in the earlier experiment is very pronounced, however, as the losses begin to decrease significantly in higher wavelengths at above 700 °C. The losses at 950 nm appear to decrease to -25 dB/10 m. The wavelengths from 764-875 nm also show this effect, but it is much more pronounced as the wavelength increases. This “improvement” in the fibers is very different from what is expected, and requires additional investigation before it can be fully explained.

It seems that what is taking place is the introduction of light to the fibers from a secondary light source, the heater itself. As the heater reaches temperatures in the range of 750 °C it is likely emitting photons in the infrared wavelength range, some of which end up travelling through the fibers and resulting in the effect described above. The photons would have to enter the fiber at just the right angle to totally internally reflect and remain in the fiber, as shown in

Figure 30, below. The photon on the left simply passes through the fiber, while the one on the right is totally internally reflected and adds to the signal in the fiber. In conversations with Luna on this subject, David Hawn was told that this effect is negligible (Hawn). The major difference here is that we are testing multi-mode rather than single-mode fibers, and this likely has an effect on the ability of the photons to totally internally reflect, resulting in a non-negligible effect for multi-mode fibers.

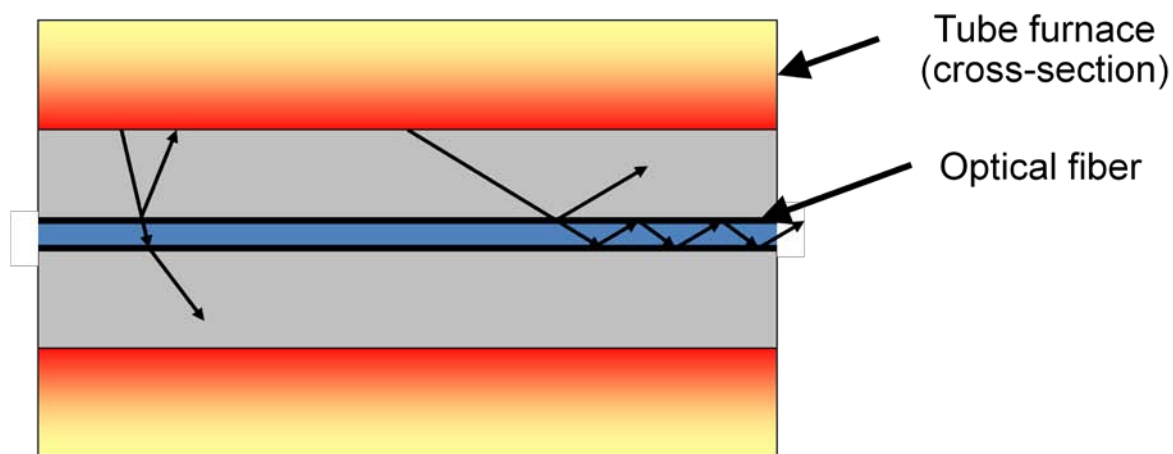


Figure 30: Introduction of Light from Secondary Source in Fibers

In a previous study similar to the one conducted in this Thesis, Oikari et al showed that the introduction of light from a furnace has a significant effect on the signal, particularly at high temperatures and high wavelengths (Oikari, Laurila and Hernberg). Figure 31, below, shows that in the 700-1100 °C range the effect does in fact increase with wavelength, just as was observed in Figure 29, above.

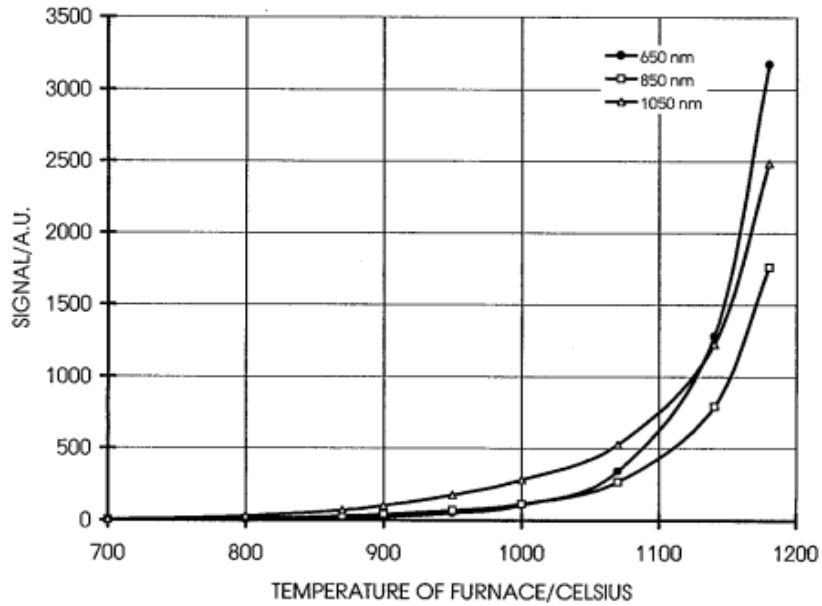


Fig. 3. Variation of the secondary source radiation signal with temperature at 650-, 850-, and 1050-nm wavelengths.

Figure 31: Variation of Secondary Source Radiation Signal, Oikari Study

It seems that introduction of light from a secondary source is likely the explanation for the aberrations that have been observed in the experiments to date. This will need to be tested further, so that the full effect of this secondary light source can be understood and accounted for in future testing. A simple method will be used to determine whether this is indeed the effect that is being observed. The fiber will be heated just as described in previous experiments, but at various points during the test the light source will actually be turned off, and the change in the signal will be observed. If the heater is actually introducing light to the fibers there should be a noticeable amount of light still being detected at high temperatures even when the source is turned off. This light can then be subtracted to determine the actual losses in the fibers more accurately.

5.1.2 Lessons Learned from Optical Testing

The optical testing of the silica fibers at high temperature has provided some important lessons learned for the future of fiber testing in the lab. The first important lesson learned is that the fibers do appear to have an effective operating range up to around 550-600 °C at which minimal losses occur in the fiber. This is particularly encouraging following the previous study in which losses increased rapidly at temperatures exceeding 200 °C, and helps to validate the decision to test these fibers for their applications in nuclear reactor environments. At the same time, increasing the temperature above this range clearly has a strongly negative effect on the fibers. It is in this range that the effects of diffusion of the dopant, crystallization of the fiber, and softening of the core likely begin to take effect. Further study will be necessary to break out these individual effects, and understand what is causing the losses in the fiber in this range, but these results are expected, as described in the literature in the Background section above. The second important lesson is that the introduction of light from the heater itself seems to have a very pronounced effect in the fiber, and this will need to be explained and accounted for in future testing. Further experiments will be conducted with the prototype furnace to better understand this effect, and steps will be taken to mitigate it in the construction of the final heater design if necessary.

5.2 Physical Performance of Silica Fibers

In addition to the optical performance described above, an important component of the fiber performance is their physical strength and durability. As described in the Background section, traditional fiber coatings typically can survive to a maximum of 385 °C, and beyond this

temperature metallic coatings must be utilized. In the case of the silica fibers tested here, which utilize a high-temperature Polymicro coating, the coating does indeed burn off during testing in the 550 °C range. The result is that the fibers become extremely brittle, and will break under any significant stress. As pictured in Figure 28 and Figure 29, the fibers become first brown, then black as the coating burns off, and finally clear once it has been fully removed. In Figure 28 the fiber was unable to be removed from the heater without breaking, and is actually broken in the middle though it is nearly impossible to see in the photo. This embrittlement has the potential to severely limit the reliability of these fibers in instrumentation applications, particularly in reactor environments in which the survivability of the instrumentation is a crucial safety matter.

5.3 Summary

Overall the prototype has provided promising results for the silica fiber testing that was performed. Once the light source was repaired, and fiber connectors were added, the data collected from the experiment was very useful. In this initial testing, the optical properties of the fibers have been shown to be much more resilient to temperature than expected from previous studies. The fibers show that they are able to successfully operate at temperatures up to 550 °C without significant decrease in efficiency. As the temperature is increased further, however, the fibers begin to degrade quickly, and attenuation increases, with the greatest attenuation occurring at lower wavelengths and decreasing as the wavelength increases. This effect, though promising, may be in large part explained by secondary light source effects, rather than any beneficial aspect of the fibers. More testing is required to determine the causes of these effects, and to verify the repeatability of them, but this initial work has provided justification both for future studies of

silica fibers at temperatures in the range tested here, and of sapphire fibers which will be necessary to reach temperatures exceeding 900 °C.

CHAPTER 7: CONCLUSIONS AND FUTURE WORK

7.1 Conclusions

As described in the Analysis section, above, one of the main conclusions that can be drawn from this study is that silica and sapphire fibers are both viable options at high temperature, though they have very different applicable ranges, and further study of both fibers for reactor environments is justified. This is encouraging, as further work continues to be done in preparation for the construction of two new furnaces, one to test each type of fiber. In addition, the construction of the prototype has yielded important information regarding the challenges as well as successes of the current design. These lessons have resulted in the decision to move forward with the construction of the high temperature furnace, the design of which has been determined to be viable, though still somewhat incomplete. An important lesson learned in the construction of the prototype furnace is that flexibility of the design is important, and some design decisions will need to be made once progress has begun to be made in building the furnace. The overall design is sound, however, and construction is set to begin very soon.

7.2 Future Work

7.2.1 Short Term

In the short term, there are two directions that will be pursued in future work. The first is that data will continue to be collected using the prototype furnace, as the silica fibers are further

characterized before they are later tested in the silica fiber furnace that will be constructed this summer. There is much more to be understood about what is causing the attenuation observed at high temperatures, and how the fibers withstand sustained time at temperature as well. In addition, construction is ready to begin on the high temperature furnace, and this will begin in earnest this summer, with testing in the lab, and later at the OSU Research Reactor soon to follow.

7.2.2 Long Term

Long term goals for this project, once sapphire fibers have been characterized in a high temperature, radiation environment, include the fabrication and testing of sensors, such as FBG sensors, in the fibers. The survivability of such sensors will be a completely different issue in this harsh environment than the survivability of the bulk fiber itself. This is because the competing effects of radiation damage and annealing will not have the ability to repair the grating structure etched in the fibers in the same way that it might repair damage in the bulk fiber. Once sensors are successfully created and characterized in this environment, attention can be turned to creating a sensor network utilizing these sensors, and providing distributed in-core temperature measurements.

BIBLIOGRAPHY

ASTM International. "Manual On the Use of Thermocouples in Temperature Measurement."
1993.

ASTM. "Standard E 1614-94." 2004.

Bhatia, V. "Optical fibre based absolute extrinsic Fabry-Perot interferometric sensing system."
Measurement Science and Technology (1996): 58.

Grobncic, Dan and Stephen J Mihailov. "Sapphire Fiber Bragg Grating Sensor Made Using
Femtosecond Laser Radiation for Ultrahigh Temperatures." IEEE Photonics Technology
Letters November 2004: 2505-2507.

Han, Ming. "Signal-processing algorithm for white-light optical fiber extrinsic Fabry-Perot
interferometric sensors." Optics Letters (2004): 1736-1738.

Hawn, David. John Hanson's Thesis Defense John Hanson. 14 May 2010.

MHI. Robust Radiator Modules. 2009. 2010 <<http://www.mhi-inc.com/PG3/robust-radiator.html>>.

Oikari, Risto, Toni Laurila and Rolf Hernberg. "High-temperature effects in flourine doped,
fused synthetic silica fibers." Applied Optics 20 July 1997.

Othonos, Andreas and Kyriacos Kalli. Fiber Bragg Gratings. Boston: Artech House, 1999.

Shiota, Takao and Hiroshi Hidaka. "High-Temperature Effects of Aluminum-Coated Fiber." Journal of Lightwave Technology (1986): 1151-1156.

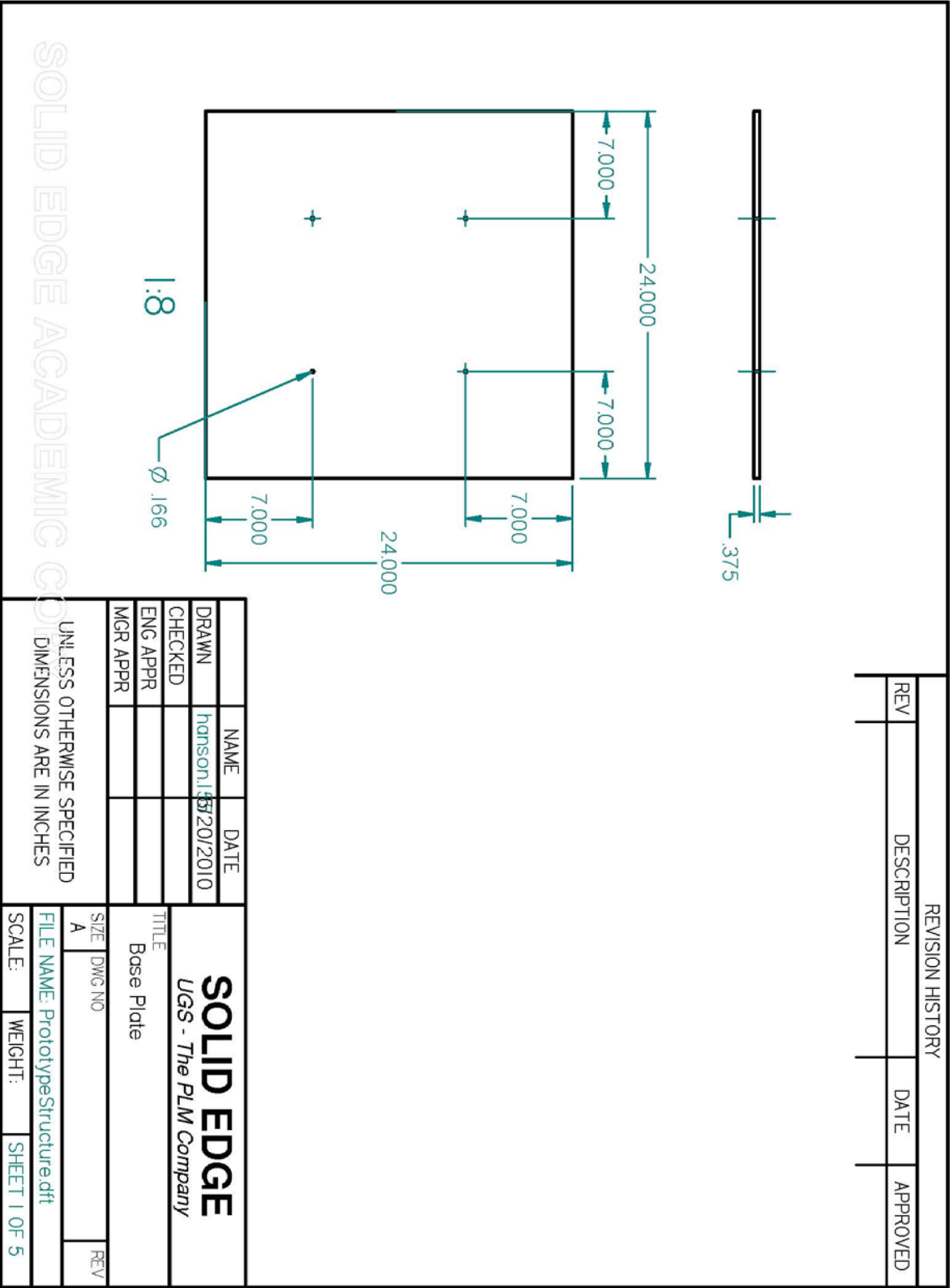
Toossi, R and D Modarress. "Radiation and Temperature Survivability of Multimode Step-Index Fluorine-Doped Silica Fibers." IEEE Transactions on Nuclear Science October 1991: 985-993.

Wang, Anbo, Yizheng Zhu and Gary Pickerell. "Optical Fiber High-Temperature Sensors." Optics and Photonics News March 2009: 27-31.

Zhu, Yizheng and Zhengyu Huang. "Sapphire-fiber-based white-light interferometric sensor for high-temperature measurements." Optics Letters 1 April 2005: 711-713.

APPENDIX

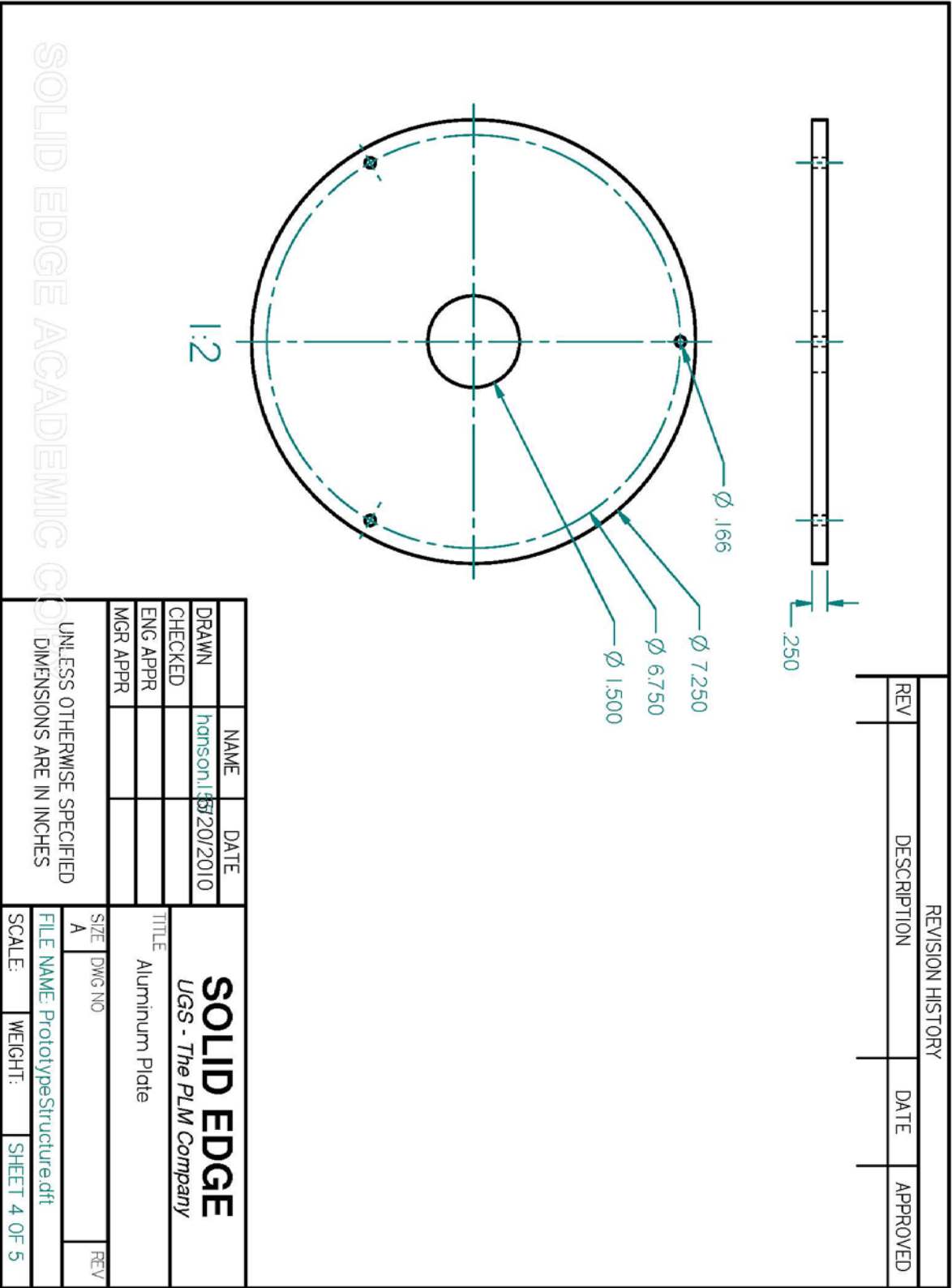
Appendix A: CAD Drawings of Initial Furnace Design



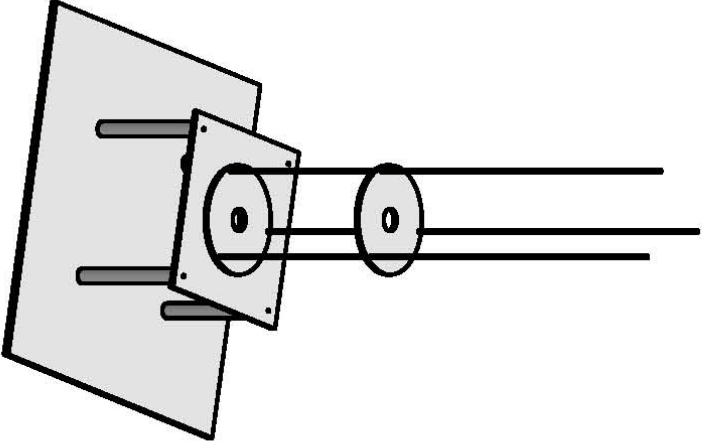
REVISION HISTORY			
REV	DESCRIPTION	DATE	APPROVED

NAME	DATE	TITLE	
DRAWN	hanson, l	SOLID EDGE	
CHECKED	5/20/2010	UGS - The PLM Company	
ENG APPR		Aluminum Bar	
MGR APPR			
UNLESS OTHERWISE SPECIFIED DIMENSIONS ARE IN INCHES		SIZE	REV
		A	
		FILE NAME: PrototypeStructure.dft	
SCALE:		WEIGHT:	SHEET 3 OF 5

SOLID EDGE ACADEMIC COPY



REVISION HISTORY			
REV	DESCRIPTION	DATE	APPROVED



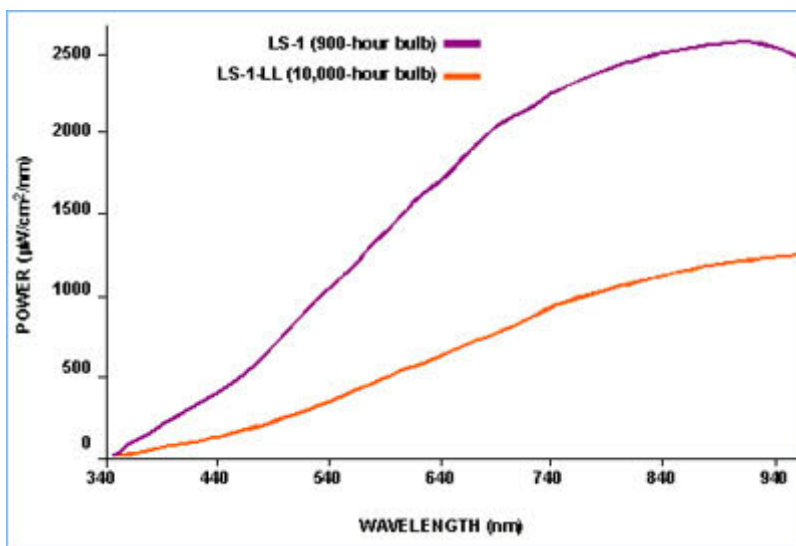
Item Number	Title	Material	Quantity
1*	3' #10-24 All-Thread Rod	Al 6061	3
2*	Base Plate	Al 6061	1
3*	Aluminum Rods	Al 6061	4
4*	Top Plate	Al 6061	1
5*	Aluminum Plate	Al 6061	2

NAME	DATE	SOLID EDGE <i>UGS - The PLM Company</i>
DRAWN	Hanson, J. 5/20/2010	
CHECKED		
ENG APPR		
MGR APPR		
TITLE Assembly		
SIZE A	DWG NO	REV
FILE NAME: PrototypeStructure.dft		
SCALE:	WEIGHT:	SHEET 5 OF 5

UNLESS OTHERWISE SPECIFIED
DIMENSIONS ARE IN INCHES

SOLID EDGE ACADEMIC COLLEGE

Appendix B: Ocean Optics LS-1 Manufacturer's Specifications



Spectral range:	360-2500 nm
Dimensions:	9.0 cm x 5.0 cm x 3.2 cm; 3.5" x 2.0" x 1.25"
Power input:	12 VDC/800 mA; 7-20 VDC/0.4-2 amps
Power output:	6.5 watts
Bulb life:	900 hours (standard); 10,000 hours (long-life)
Bulb color temperature:	3100 K (900-hour bulb); 2800 K (10,000-hour bulb)
Output to bulb:	5 volts/1.3 amps
Output regulation:	0.2% voltage
Time to stabilized output:	~20 minutes
Stability:	decay rate is ~0.1%/hour of the output power
Bulb output:	7400 foot-candles (7.4MSCP)
Internal filter accessory:	BG-34 conversion filter
External filter slot:	accepts filters up to 3 mm thickness
Spectral attenuation:	50%, 75% and 99% with PTFE disk accessories
Connector:	SMA 905
* If used with an Ocean Optics spectrometer, the LS-1's practical spectral range is limited to the spectral response of the detector -- for the USB2000, approximately 1100 nm (1.1 µm).	

Source: Manufacturers Website (<http://www.oceanoptics.com/products/lsl.asp>)

Appendix C: Ocean Optics USB 2000 Manufacturer's Specifications

Physical	
Dimensions:	89.1 mm x 63.3 mm x 34.4 mm
Weight:	190 grams
Detector	
Detector:	Sony ILX511 linear silicon CCD array
Detector range:	200-1100 nm
Pixels:	2048 pixels
Pixel size:	14 μm x 200 μm
Pixel well depth:	~62,500 electrons
Sensitivity:	75 photons/count at 400 nm; 41 photons/count at 600 nm
Optical Bench	
Design:	f/4, Symmetrical crossed Czerny-Turner
Focal length:	42 mm input; 68 mm output
Entrance aperture:	5, 10, 25, 50, 100 or 200 μm wide slits or fiber (no slit)
Grating options:	14 different gratings, UV through Shortwave NIR
HC-1 grating option:	No
Detector collection lens option:	Yes, L2
OFLV filter options:	OFLV-200-850; OFLV-350-1000
Other bench filter options:	Longpass OF-1 filters
Collimating and focusing mirrors:	Standard or SAG+
UV enhanced window:	Yes, UV2
Fiber optic connector:	SMA 905 to 0.22 numerical aperture single-strand optical fiber
Spectroscopic	
Wavelength range:	Grating dependent
Optical resolution:	~0.3-10.0 nm FWHM
Signal-to-noise ratio:	250:1 (at full signal)
A/D resolution:	12 bit
Dark noise:	3.2 RMS counts
Dynamic range:	2 x 10 ⁸ (system); 1300:1 for a single acquisition
Integration time:	3 ms to 65 seconds
Stray light:	<0.05% at 600 nm; <0.10% at 435 nm
Corrected linearity:	>99.8%
Electronics	
Power consumption:	90 mA @ 5 VDC

Data transfer speed:	Full scans to memory every 13 ms with USB 2.0 or 1.1 port, 300 ms with serial port
Inputs/Outputs:	No
Analog channels:	No
Auto nulling:	No
Breakout box compatibility:	No
Trigger modes:	3 modes
Strobe functions:	Yes
Gated delay feature:	Yes
Connector:	10-pin connector
Computer	
Operating systems:	Windows 98/Me/2000/XP, Mac OS X and Linux with USB port; Any 32-bit Windows OS with serial port
Computer interfaces:	USB 2.0 @ 12 Mbps; RS-232 (2-wire) @ 57.6 K baud
Peripheral interfaces:	I2C inter-integrated circuit

Source: Manufacturers Website (<http://www.oceanoptics.com/Products/usb2000.asp>)